REPORT NO. FR-79-73-999
HAC REF. NO. E2380

DATA SYSTEMS GROUP
HUGHES
HUGHES AIRCRAFT COMPANY

HIGH ENERGY OPTICAL RESONANCE TRANSFER LASER STUDY

HUGHES AIRCRAFT COMPANY
CULVER CITY, CALIFORNIA 90230

AUGUST 1979

Final Technical Report
Volume I, Laboratory Experiments

The views and conclusions contained in this document are those of the authors and should not be interpreted as necessarily representing the official policies, either expressed or implied of the Defense Advanced Research Projects Agency or the U.S. Government.

SPONSORED BY
Defense Advanced Research Projects Agency
DARPA Order No. 2062, Amendment No. 19

MONITORED BY
Mr. Wayne Whitney, NRL Code 5540, under
Contract No. N00173-78-C-0470

CONTRACT EFFECTIVE DATE: 24 July 1978
CONTRACT EXPIRATION DATE: 24 August 1979

SECURITY CLASSIFICATION OF THIS PAGE (When Data Entered)

REPORT DOCUMENTATION PAGE

READ INSTRUCTIONS BEFORE COMPLETING FORM

1. REPORT NUMBER

2. GOVT ACCESSION NO.

3. RECIPIENT'S CATALOG NUMBER

4. TITLE (and Subtitle)
High Energy Optical Resonance Transfer Laser Study, Volume I, Laboratory Experiments

5. TYPE OF REPORT & PERIOD COVERED
Final Technical Report
24 July 1978 to 23 June 79

6. PERFORMING ORG. REPORT NUMBER
FR-79-73-999

7. AUTHOR(s)
P. Baily, J. Finzi, C. Lovejoy, and J. Wang

8. CONTRACT OR GRANT NUMBER(s)
N00173-78-C-0470
DARPA Order-2062

9. PERFORMING ORGANIZATION NAME AND ADDRESS
Hughes Aircraft Company
Centinela and Teale Streets
Culver City, CA 90230

10. PROGRAM ELEMENT, PROJECT, TASK AREA & WORK UNIT NUMBERS
Darpa Order No. 2062
Amendment No. 19

11. CONTROLLING OFFICE NAME AND ADDRESS
Defense Advanced Research Projects Agency
1400 Wilson Boulevard
Arlington, VA

12. REPORT DATE
August 1979

13. NUMBER OF PAGES
75 (82 p.)

14. MONITORING AGENCY NAME & ADDRESS (if different from Controlling Office)
Naval Research Laboratory
4555 Overlook Ave., S.W.
Washington, D.C.

15. SECURITY CLASS. (of this report)
Unclassified

15a. DECLASSIFICATION DOWNGRADING SCHEDULE

16. DISTRIBUTION STATEMENT (of this Report)
None

DISTRIBUTION STATEMENT A
Approved for public release;
Distribution Unlimited

17. DISTRIBUTION STATEMENT (of the abstract entered in Block 20, if different from Report)
None

HAC-FR-79-73-999-VOL-1
HAC-REF-E2589-VOL-1

18. SUPPLEMENTARY NOTES
None

19. KEY WORDS (Continue on reverse side if necessary and identify by block number)
Optical Pumping
HF Lasers
Transfer Lasers

20. ABSTRACT (Continue on reverse side if necessary and identify by block number)
This report describes characterization experiments investigating an HF intramolecular Optical Resonance Transfer Laser (ORTL), with variation in pump laser characteristics, ORTL volume, and ORTL medium composition, pressure, and flow velocity. Input coupling, conversion, and overall efficiency were characterized in several different geometries. Maximum values of 83 per cent for conversion efficiency and 29 per cent for overall efficiency were observed. Initial temporal measurements revealed no dynamic feedback interaction in the intra-cavity configuration. Diffraction limited ORTL beam quality was observed.

DD FORM 1 JAN 73 1473 EDITION OF 1 NOV 65 IS OBSOLETE

SECURITY CLASSIFICATION OF THIS PAGE (When Data Entered)

409 084

SUMMARY

This report covers the activity in the second half of the program. During the first half of the program a number of Optical Resonance Transfer Laser (ORTL) systems were investigated. This work was discussed in detail in the Mid-Term Technical Report, and included investigation of the HF/DF, HF/HCl and HF/HCN intermolecular ORTL systems as well as the intramolecular HF ORTL system. As a result of that work and potential efficiency estimates, the second half of the program concentrated on the intramolecular HF ORTL system. The effort reported here included a Characterization Task, a Chemical Laser/ORTL Dynamics Task, and an ORTL Beam Quality Task. The results of these experimental efforts are discussed in Volume 1. The activity in a concurrent Scaling Analysis Task is discussed in Volume 2.

Three different ORTL geometries were used in the Characterization Task and systematic variations in ORTL pressure, flow velocity, and medium composition were made. Different ORTL cell volumes were utilized and the chemical laser pump beam characteristics were varied. The highest measured ORTL output power was 135 watts corresponding to a 29 percent overall efficiency of conversion of available pump power to coherent ORTL power. A more fundamental quantity is the conversion efficiency of absorbed power to coherent ORTL power. The maximum observed value for this quantity was 83 percent.

Initial temporal characterization of the intracavity ORTL configuration was performed. The ORTL and chemical laser outputs were monitored and the chemical laser output temporal characteristics were not affected by the presence of an absorbing ORTL medium. The ORTL output characteristics were similar to those from an extracavity ORTL operating at a similar level above threshold. Initial ORTL output beam quality measurements were made and diffraction limited performance was observed.

PREFACE

The work presented in this report was performed simultaneously with work at Hughes on DF ORTL systems sponsored by Air Force Avionics Laboratory under Contract F33615-78-1477. The authors wish to acknowledge the mutual influence of these two contracts upon each other. This report was authored by P. Baily, J. Finzi, C. Lovejoy, and J. Wang. P. Baily was the program manager. The experiments were performed with the assistance of R. Shimazu and L. Williams. The authors would also like to acknowledge valuable discussions with K. Hui, G. Holleman, L. Marabella, F. Mastrup, and M. Mann.

CONTENTS

LIST OF ILLUSTRATIONS

LIST OF ILLUSTRATIONS (Continued)

LIST OF TABLES

1.0 INTRODUCTION

High energy chemical lasers should exhibit near diffraction limited beams in order to generate maximum target irradiance levels at minimum size and weight. Because of problems associated with maintaining the chemical laser medium homogeneity and with the complexity of the resonator design of the cylindrical chemical laser configuration, it is difficult to achieve near diffraction limited beams directly. One promising approach to solving this problem is to use the high energy chemical laser as an optical pump for exciting a second laser applying the Optical Resonance pumped Transfer Laser (ORTL)* technique. With this technology, the original stringent mode and medium requirements on the high energy chemical laser are significantly relaxed and the cylindrical chemical laser resonator arrangement simplified. Because the role of the chemical laser is reduced to that of a source of optical power only, multi-mode characteristics of the chemical laser are no longer detrimental. The output beam control function of the total laser system is transferred in this new approach to the second laser, the ORTL. The two functions of the laser system, to generate power and to concentrate that power into a highly confined beam, are separated. Of course, the premise that is fundamental to the ORTL approach to high energy laser system optimization is that each of the two functions can be solved separately in a more optimum way, so that better far field target irradiance can be achieved by the chemical laser/ORTL system than by directly focusing the same primary chemical laser power onto the target.

The intermolecular ORTL technique as originally demonstrated made use of two molecules, a donor and an acceptor, as the active ORTL medium, flowing in a helium diluent. The chemical laser (DF) served as the optical pump exciting the donor (DF) molecules in the ORTL cell. This donor then collisionally transferred its energy to an acceptor (CO_2) molecule which

*J.H.S. Wang, J. Finzi, and F.N. Mastrup, Appl. Phys. Lett. 31, 35 (1977).

then became the active laser molecule for the ORTL. Subsequent to the original DF/CO_2 (10.6 μ) demonstration, this technique was extended to DF/HBr (4.1 μ) and DF/N_2O (10.8 μ) systems.* In addition, a similar process in which only one molecule (DF) was present in the ORTL cell was demonstrated.** In this intramolecular DF ORTL system, the DF molecule served as both donor and acceptor. The DF molecules absorbed on the transition of the chemical pumping laser and excitation from one vibrational band to a higher band was achieved. Then, the energy was redistributed among the rotational levels of each vibrational band as the systems approached rotational equilibrium. As this occurred, population inversions on non-pumped vibration-rotational transitions were achieved and laser oscillation occurred. There was, of course, a slight wavelength shift.

The issues that must be addressed before either ORTL approach can become a practicable and preferred solution to the high energy cylindrical laser beam control problem are whether very high conversion efficiency from multi-line HF or DF chemical laser power to ORTL power is achievable, and whether adequate medium homogeneity to permit the extraction of near diffraction limited beams at realistically scaled output power levels is possible. In order to gain the detailed technical understanding with which to address these issues, the High Energy ORTL Study was performed. Because the primary interest for DARPA applications is in HF lasers, it was decided that the program would concentrate on HF laser pumped systems. Prior work had dealt exclusively with DF laser pumped systems.

The primary objective of this program was the development of a detailed understanding of the ORTL technique through properly chosen laboratory experiments and analysis of the results. This study was an experimental one, not an analytical one. An associated goal of the program was the application of the attained understanding to the assessment of the potential of the technique for DARPA application through scaling analysis.

---

*Hughes IR&D, 1978

**4.3 Micrometer Laser Demonstration Experiment, Contract No. N00173-77-C-0174, Final Report, December, 1977.

The program was structured with five tasks. The initial task was an experimental screening of candidate ORTL systems with the objective of selecting a single system for concentrated investigation during the remainder of the program. Three new ORTL systems were demonstrated in that task. The intramolecular HF ORTL and the intermolecular HF/DF and HF/HCN ORTL systems were demonstrated. The results of this task were reported in the Mid-Term Technical Report* and will not be discussed here. Because intramolecular rotational redistribution is much faster than intermolecular V-V collisional energy transfer, the intramolecular ORTL possesses an inherent efficiency advantage. The expected efficiency advantage was observed in the Screening Task experiments, and the HF intramolecular ORTL system was selected as the one to be studied during the second half of the program.

During the second half of the program three experimental tasks were completed. These were the HF ORTL Characterization Task, the Chemical Laser/ORTL Dynamics Task, and the ORTL Output Beam Quality Task. The results of these efforts are discussed in Volume I. In addition to the experimental work, a Scaling Analysis Task was completed; this effort is discussed in Volume II. The experimentally achieved overall efficiency (ORTL coherent power produced from available pump power) of 29 percent is indicative of the even higher efficiencies predicted in high energy systems. This experimental result is a significant part of the answer to the efficiency question. The beam quality issue was also investigated in as much as the present laboratory apparatus would allow. Diffraction limited ORTL output was observed, but the sensitivity to medium inhomogeneity was minimal.

---

*High Energy Optical Resonance Transfer Laser Study, Contract No. N00173-78-C-0470, Mid-Term Technical Report, January, 1979.

2.0 HF INTRAMOLECULAR ORTL CHARACTERIZATION

2.1 BACKGROUND

As a result of analysis of the Screening Task experiments, the HF intramolecular ORTL system was selected for concentrated investigation in the second half of the program. The prime reason for this choice was the inherent high efficiency of the intramolecular ORTL compared to the intermolecular ORTL. Because rotational equilibration rates are more rapid than intermolecular V-V collisional transfer rates, the losses in an intramolecular ORTL are expected to be smaller than in the intermolecular ORTL. This expectation manifested itself in the Screening Task experiments.

Two configurational families have been identified for potential use in high energy chemical laser/ORTL systems. These are the extra-cavity and intra-cavity configurations. In the extra-cavity configuration the ORTL cell is external to the chemical laser optical resonator. The chemical laser output illuminates the ORTL cell and pumps the active molecules. The overall efficiency is determined by the efficiency of absorption of the incident pump power (input coupling efficiency) and the efficiency of conversion of absorbed power to coherent ORTL power (conversion efficiency). In the intra-cavity configuration the ORTL cell is placed inside a closed cavity chemical laser optical resonator. The ORTL cell provides the main outcoupling of available chemical laser power and the ORTL input coupling efficiency can be very large.

In future applications the intra-cavity configuration will probably be preferred because of its potentially high efficiency. However, implementation is significantly more complex because of the coupling between ORTL processes and chemical laser power extraction. The objective of the present study was understanding of ORTL kinetic processes and the extra-cavity configuration was selected for most of the present work because of its conceptual simplicity. Intra-cavity experiments were, however, implemented for the Chemical Laser/ORTL Dynamics task discussed in Section 3.0.

The emphasis in the Characterization Task was on the pursuit of physical understanding through a series of parametric studies and subsequent demonstration of high overall efficiency. Experimental apparatus improvements initiated at the outset of this task are discussed in Section 2.2. Several new ORTL nozzles were fabricated; the results obtained with these nozzles are discussed in Section 2.4. Parametric studies varying ORTL HF mole fraction, gas pressure and flow velocity were conducted for several chemical laser operating conditions. Both closed cavity and 5 percent outcoupling ORTL resonators were used. Pump laser power and spectral distribution, and ORTL output power and spectral distribution were measured. In Section 2.5, a new extracavity configuration, the multiple pass cell, which increases the input coupling efficiency while preserving low ORTL oscillation threshold is described. This configuration produced the highest overall efficiencies observed to date in any ORTL experiment.

2.2 APPARATUS IMPROVEMENTS

Analysis of the Screening Task results indicated several improvements to the existing apparatus which could potentially lead to increased efficiencies. The Screening Task apparatus is depicted in Figure 1. The outcoupled beam from a combustion driven HF chemical laser was cylindrically focused to a 2.3 cm x 0.38 cm cross-section at the optical pumping zone. A room temperature HF/He gas mixture entered the pumping zone through a 3 mm x 6 cm nozzle with a velocity of 5×10^3 cm/sec. Gas pressure was varied from 40 torr to 110 torr, and the HF mole fraction was varied from one to three percent. The nozzle was rotated at a 20 degree angle relative to the chemical laser optical axis so that the 2.3 cm pump beam could cover the entire 6 cm length of the gas flow as indicated in Figure 1. A mirror placed at the opposite end of the cell refocused the pump beam back onto the pumping zone to enhance the pumping processes. The resonator for the optically pumped HF laser consisted of a flat total reflector and a 3 meter radius of curvature concave outcoupler separated by 75 cm. The optical axis was oriented along the 6 cm nozzle dimension. A thermocouple placed 1.2 cm downstream of the exit of the interaction zone measured the gas temperature

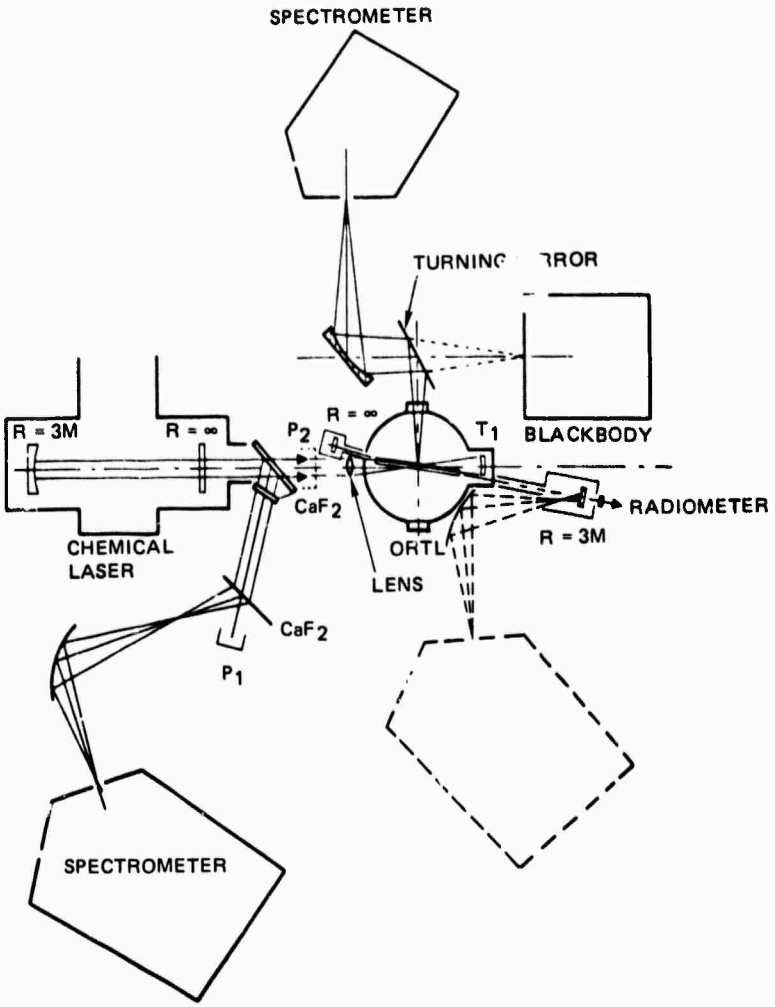

Figure 1a. Screening Task experiments – Apparatus configuration.

Figure 1b. Rotated ORTL cell.

rise allowing the power deposited in the gas to be computed. A scanning spectrometer was used to determine the spectral distribution of the pump laser and the optically pumped HF laser. The absorption efficiency of the apparatus would be increased if the absorption path length were increased. Therefore, a 6 mm x 6 cm nozzle was fabricated for use in the rotated ORTL cell. One also would expect an increase in overall efficiency if the pump irradiance were increased. Therefore, a 3 mm x 3 cm nozzle was fabricated for use with a smaller pump beam.

In order to observe the maximum achievable ORTL efficiency, a closed cavity ORTL resonator was also designed and fabricated. It consisted of two mirrors made of molybdenum which has a high thermal conductivity and low thermal expansion coefficient. Thermocouples were embedded along the side and back of each mirror so that the heating rate in each mirror could be recorded and the extracted ORTL power computed. The mirrors were thermally isolated by being held in a spider mount with four stainless steel pins. The calorimetry method used in this test was described by Hass, et al.*

One mirror was a concave spherical total reflector with a three meter radius of curvature and the other was flat. They were separated by ninety centimeters in most experiments. Each mirror had a diameter of 1.25 inches and a thickness of one inch. These dimensions were determined so that the mirror heat capacity was large enough to have a small heating rate (0.67 degree/sec for a 100 watt ORTL), but thin enough to have a fast thermal response time (less than one second).

A Ag/ThF_4 coating was applied to each mirror and the reflectivity (approx. 98.8 percent) measured. After weighing the mirror, iron/constantan thermocouples were affixed to the back and side of each mirror with a small amount of high thermal conductivity epoxy. Reference thermocouples were maintained in a water bath and the mirror temperature determined from a differential voltage measurement. The mirror temperature during a typical experiment is shown schematically in Figure 2. During the

*M. Hass, J. W. Davisson, P. H. Klein and L. L. Boyer, J. Appl. Phys. 45, 3959 (1974).

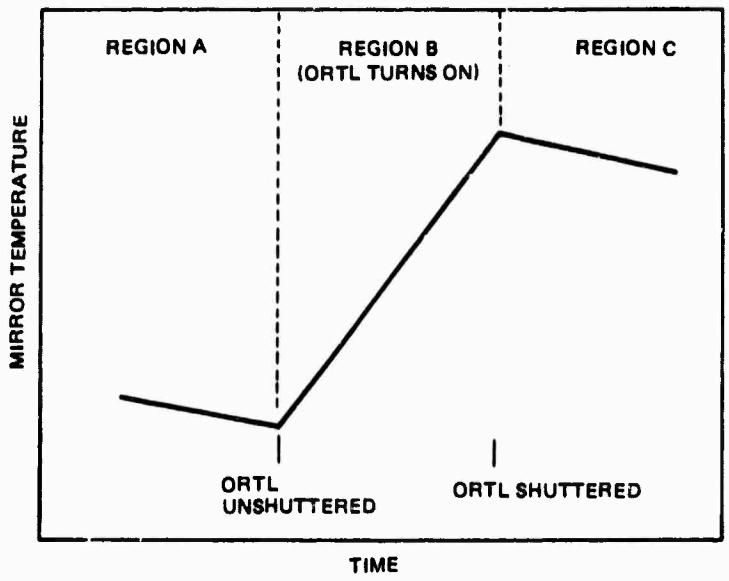

Figure 2. Closed cavity power measurement.

period denoted "A." the ORTL cavity was spoiled by a mechanical shutter. The chemical laser and ORTL flow were turned on and stabilized. Unshuttering the ORTL cavity resulted in the temperature rise in region "B" in Figure 2. The ORTL was then shuttered. and in region "C" the cooling of the mirror is apparent. The cooling by convection and radiation which occurred during periods A and C also occurred during period B. Since the cooling rate was proportional to the temperature difference between the mirror and its surroundings. a correction. which was the average of the cooling rates before and after heating, was applied to the observed slope during period B. This corrected slope was then used to compute absorbed power. The cooling correction was typically 0.4 to 0.9 watt. This correction was less than 2 percent at high powers.

2.3 OPTICAL ABSORPTION MEASUREMENT

In the Screening Task. total power absorption in the ORTL medium was obtained from the sum of ORTL output power and the heat deposited in the ORTL gas. The latter was computed from the temperature rise as measured by a thermocouple placed 1.2 cm downstream of the exit of the pump interaction zone. Because of the importance of the absorbed power for determination of input coupling and power conversion efficiencies, an experiment was

undertaken to confirm the values obtained from the thermocouple measurements. Optical power absorption measurements were chosen for this purpose and were performed under experimental conditions similar to those for which the best efficiencies had been achieved. In this single pass optical power absorption measurement, two signals were continuously monitored, each representing a fixed fraction of the pump laser beam. The first signal was generated by a CaF_2 beam splitter placed before the ORTL cell. The second signal was generated by another beam splitter placed after the ORTL cell. From the ratios of these two signals with and without gas in the ORTL cell the transmittance and the input coupling efficiency of the ORTL cell were determined. The gas temperature rise and the pump laser power were also monitored during these experiments and input coupling efficiency determined from these quantities. Input efficiencies derived from these two methods are shown in Figure 3 as a function of HF mole fraction in the ORTL medium. They are within 15 percent of each other. This is well within the estimated experimental errors. From these observations it was concluded that the efficiencies derived from the measured gas temperature rise are correct and this method could be confidently used for the remainder of the experiments. To study the ORTL medium uniformity along the 6 cm gain length, four thermocouples were installed. One was at the center of the region, one was placed 1.5 cm on each side of the center and the fourth was placed 2.5 cm from the center. They were all located 1.2 cm downstream of the ORTL interaction zone exit.

2.4 EXTRA-CAVITY ROTATED ORTL CELL EXPERIMENTS

Ten test series were conducted as shown in Table 1. As indicated, chemical laser power was varied as were the ORTL nozzle dimensions and the ORTL medium gas dynamic parameters. The pump laser power indicated is that which illuminates the ORTL cell. The beam path optics (CaF_2 windows, focusing lens, etc.) have resulted in degradation of the 700-800 watt output of the chemical laser to the values shown. (Anti-reflection coated optics were not used in these experiments.) Within each test series, the ORTL medium composition was varied. Detailed test results are tabulated in Table 2. The pump laser characteristics and ORTL conditions are

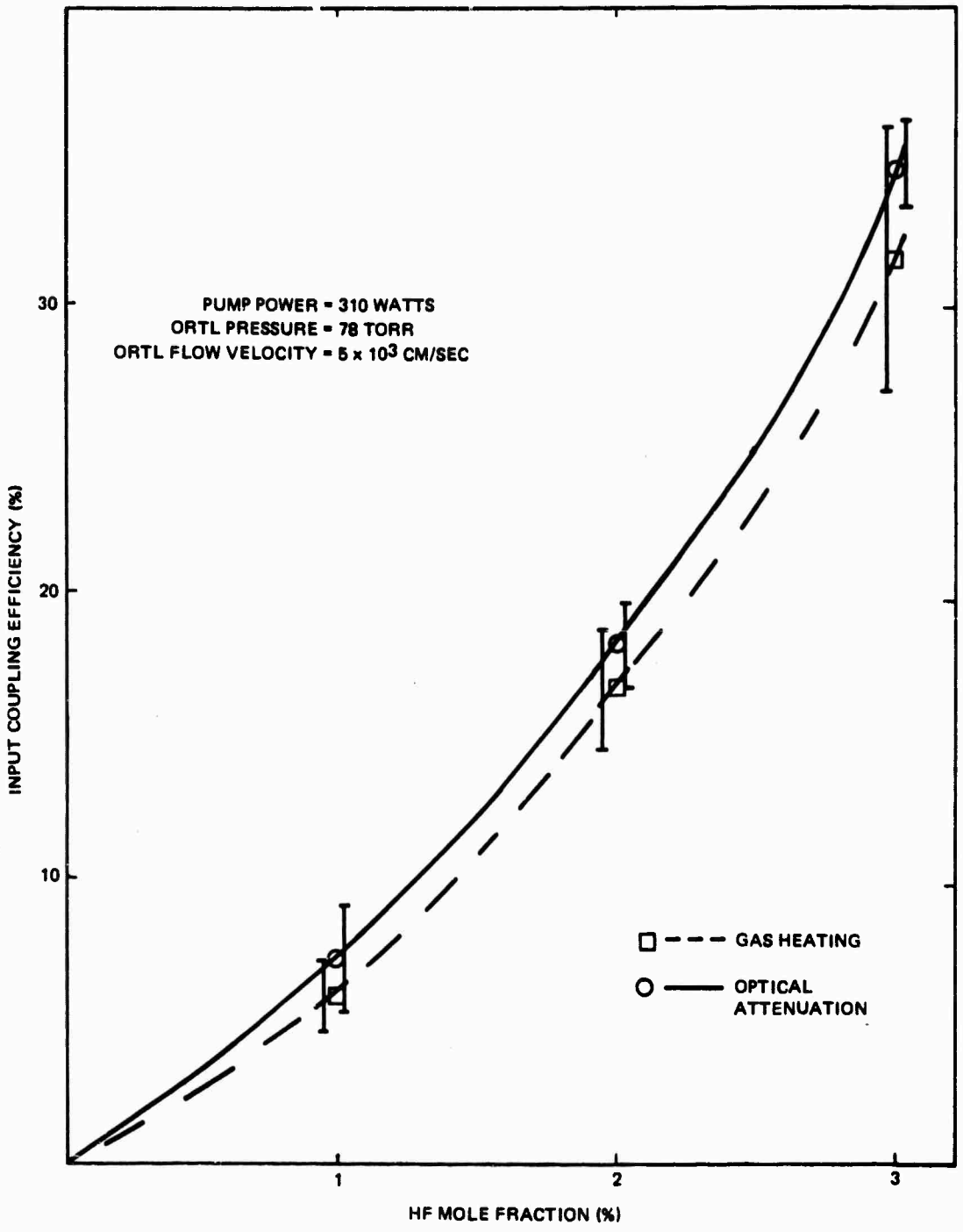

Figure 3. Comparison of alternate input coupling efficiency measurement techniques.

TABLE 1. ROTATED ORTL CELL EXPERIMENTS

Test Series	ORTL Resonator	ORTL Nozzle (cm)	Pump Laser Power (watts)	ORTL Pressure (torr)	ORTL Flow Velocity (cm/sec)
I	5% Outcoupling	0.3 X 6	550	76	5×10^3
II	Closed cavity	0.3 X 6	550	76	5×10^3
III	Closed cavity	0.3 X 6	480	76	5×10^3
IV	5% Outcoupling	0.6 X 6	418	76	5×10^3
V	Closed cavity	0.6 X 6	418	76	5×10^3
VI	Closed cavity	0.6 X 6	418	76	2.5×10^3
VII	Closed cavity	0.6 X 6	418	40	5×10^3
VIII	Closed cavity	0.6 X 6	375	76	5×10^3
IX	Closed cavity	0.6 X 6	375	110	5×10^3
X	Closed cavity	0.3 X 3	340	76	5×10^3

listed along with the measured ORTL medium temperature rises. T_1 was measured by the thermocouple located on the ORTL optical axis 1.5 cm from the center line; T_2 is on the center line; T_3 is 2.5 cm from the center line and on the opposite side from T_1. The average of these three values was used to compute the power deposition in the gas, Q_{gas}. The power deposited in the ORTL mirrors and the outcoupled power (where appropriate) were combined to yield the total absorbed power. The derived input coupling, conversion, and overall efficiencies are also listed.

The first interesting observation about this data is the spatial non-uniformity of the temperature rise in the ORTL medium. The temperature rise is primarily due to the deactivation of the HF vibrationally excited states. The excited state density depends upon the pump irradiance and its spectral distribution as well as upon the deactivation rate. The non-uniformity of the temperature rise reflects the spatial non-uniformity of the pump radiation. The temperature rise is fairly uniform in the low HF mole fraction cases such as I-1, II-1 and III-1, but not in the high HF mole fraction cases such as I-3, III-4 and IV-5. In low HF mole fraction cases, the pump power across the gain length is high enough to bleach the ORTL

TABLE 2. ROTATED ORTL CELL EXPERIMENTAL RESULTS

Test	Pump Laser Characteristics			ORTL Conditions					ORTL Temperature Rise			Q_{gas}	Extracted ORTL Power		Absorbed Pump Power	ORTL Efficiency		
	Power Cross Section (watts) (cm x cm)	Spectral Distribution $P_1(4)/P_1(5)$ $P_2(4)/P_2(5)$ $P_1(6)/P_1(7)$ $P_2(6)/P_2(7)$ (percent)		Resonator	Pressure (torr)	HF Mole Fraction	Velocity (cm/sec)	Nozzle (cm x cm)	T_1 (^oK)	T_2 (^oK)	T_3 (^oK)	(watts)	Deposited in ORTL Mirrors (watts)	Outcoupled Power (watts)	(watts)	η_{in}	η_{conv}	η_T
I-1	550 2.5 x 0.4	5.5/18.5 21.6/ 5.0	11.7/24.0 10.5/ 3.2	5% Outcoupling	76	0.01	5×10^3	0.3 x 6	93	107	115	81.9	4.5	25.6	112	0.20	0.26	0.055
I-2						0.02			227	301	287	212	2.9	17.8	232.7	0.42	0.089	0.038
I-3						0.03			280	382	353	264	1.4	10.0	275.4	0.50	0.041	0.021
II-1	550 2.5 x 0.4	5.5/18.5 21.6/ 5.0	11.7/24.0 10.5/ 3.2	Closed Cavity	76	0.005	5×10^3	0.3 x 6	24	29	32	22.1	30.4		52.5	0.095	0.58	0.055
II-2						0.01			76	109	101	74.5	42.8		117.3	0.21	0.37	0.078
II-3						0.02			213	276	251	192.5	31.8		224.3	0.41	0.14	0.058
III-1	480 2.15 x 0.38	1.5/12.0 26.0/11.0	4.0/23.0 14.0/ 5.5	Closed Cavity	76	0.003	5×10^3	0.3 x 6	10	12.5	10	8.5	17.1		25.6	0.053	0.07	0.036
III-2						0.005			24	29	20	19.0	23.9		42.9	0.089	0.56	0.050
III-3						0.01			88	104	70	68.1	44.0		112.1	0.23	0.40	0.092
III-4						0.02			217	271	171	171	31.7		202.7	0.42	0.16	0.066
IV-1	418 2.75 x 0.35	8.7/18.2 14.0/ 4.1	16.1/21.3 9.3/ 2.9	5% Outcoupling	76	0.002	5×10^3	0.6 x 6	12.3	12.5	9.7	19.2	1.9	10	31.1	0.073	0.32	0.028
IV-2						0.003			17.0	19.0	17.0	27.6	3.0	16.4	47.0	0.11	0.41	0.045
IV-3						0.005			39.5	45.0	34.5	62.5	4.8	26.0	93.3	0.22	0.33	0.073
IV-4						0.01			101.5	108.2	67	151.5	4.9	27.2	183.6	0.44	0.17	0.076
IV-5						0.015			159	167	76	231.6	2.4	16.0	250.2	0.59	0.075	0.044
V-1	418 2.75 x 0.35	8.7/18.2 14.0/ 4.1	16.1/21.3 9.3/ 2.9	Closed Cavity	76	0.003	5×10^3	0.6 x 6	15	16	10	23.0	31.1		54.1	0.14	0.52	0.073
V-2						0.005			40			61.4	34.0		95.4	0.23	0.35	0.08
V-3						0.01			107	108	73	157	52.0		208	0.50	0.24	0.126
V-4						0.15			135	142	73	245.4	31.8		277.2	0.62	0.12	0.076
VI-1	418 2.74 x 0.35	8.7/18.2 19.0/ 4.1	16.1/21.3 9.3/ 2.9	Closed Cavity	76	0.005	2.5×10^3	0.6 x 6	56	70	54	50.4	43.1		93.5	0.22	0.46	0.10
VI-2						0.01			163	197	141	145.5	48.6		194.1	0.46	0.25	0.12
VI-3						0.02			363	430	192	300	27.4		327.4	0.78	0.084	0.066
VII-1	418 2.74 x 0.35	8.7/18.2 19.0/ 4.1	16.1/21.3 9.3/ 2.9	Closed Cavity	40	0.005	5×10^3	0.6 x 6	26	31	28	29.2	25.1		54.3	0.13	0.46	0.06
VII-2						0.01			71	91	72	71.8	35.0		106.8	0.26	0.33	0.084
VII-3						0.02			183	222	151	170.7	31.7		202.4	0.48	0.16	0.077
VII-4						0.03			286	342	187	250.2	23.0		273.2	0.65	0.084	0.055
VIII-1	375 2.5 x 0.38	15/17.8 15.4	21.1/20.4 7.9/ 2.5	Closed Cavity	76	0.003	5×10^3	0.6 x 6	20.8	20.4	16	30.7	31.2		62.0	0.17	0.50	0.086
VIII-2						0.005			47.1	46	33.2	70.0	43.9		114.0	0.31	0.39	0.12
VIII-3						0.01			118	118	78	174.1	40.1		214.2	0.58	0.19	0.11
IX-1	375 2.5 x 0.38	15/17.8 15.4	21.1/20.4 7.9/ 2.5	Closed Cavity	110	0.003	5×10^3	0.6 x 6	12.2	12.8	8	27.6	43.8		71.4	0.19	0.61	0.12
IX-2						0.005			26	25.2	14	54.4	48.0		102.4	0.27	0.47	0.13
IX-3						0.01			60.6	565	29.5	124.6	23.3		147.9	0.40	0.16	0.062
X-1	340 1.5 x 0.45	11.7/14.5 18.5/ 3.8	16.5/21.5 10 / 3.1	Closed Cavity	76	0.01	5×10^3	0.3 x 3	26	103	75	29.0	32.3		61.3	0.18	0.53	0.095
X-2						0.015			54	214	154	60.8	41.4		102.2	0.30	0.41	0.12
X-3						0.02			78	302	224	86.5	40.8		127.3	0.38	0.32	0.12
X-4						0.03			118	470	361	139.4	31.6		171.0	0.50	0.19	0.093

absorbing transitions. Therefore, the temperature rise is relatively uniform even though there is some spatial non-uniformity of the pump radiation. As the HF mole fraction increases, bleaching is incomplete in some regions because of the pump spatial non-uniformity. Therefore, the temperature rise is not the same across the medium. This non-uniformity could have a serious effect on the overall efficiency because it is possible that significant positive gain is not achieved in regions where the pump intensity is low or of low J-value. This effect of pump radiation non-uniformity on overall ORTL efficiency has not been directly investigated, but should be pursued in the future.

Power extraction data obtained with the 3 mm by 6 cm cell operated at 76 torr (series I through III) are shown in Figure 4. Both outcoupled and closed cavity powers are shown. Two different test series were conducted with the closed cavity resonator and one was conducted with the outcoupling resonator. The maximum extracted power was 44 watts at an HF mole fraction of 1 percent with the remainder of the ORTL gas being helium. The maximum outcoupled power was 25 watts. Based upon the temperature and power measurements, closed cavity efficiencies were calculated. Those for Series III are shown in Figure 5. High conversion efficiencies were obtained This quantity reached 67 percent at an HF mole fraction of 0.3 percent. This low HF concentration limits the energy absorption resulting in a low overall efficiency at these conditions in this apparatus. As the HF concentration increases, raising the input coupling efficiency, the absorbed power required to reach the lasing threshold also increases resulting in lower conversion efficiency. The overall efficiency is the product of these two and reaches its peak of 9.2 percent at a 1 percent HF concentration.

The ORTL output spectrum was obtained by monitoring the scattered light from one of the resonator mirrors. The spectra at several HF concentrations in Series III are shown along with the chemical laser pumping spectrum in Figure 6. The shift to higher wavelength in the ORTL spectrum can be seen. The ORTL spectrum is much simpler than the pump laser, usually exhibiting two or less lines per band. The overall lasing bandwidth is

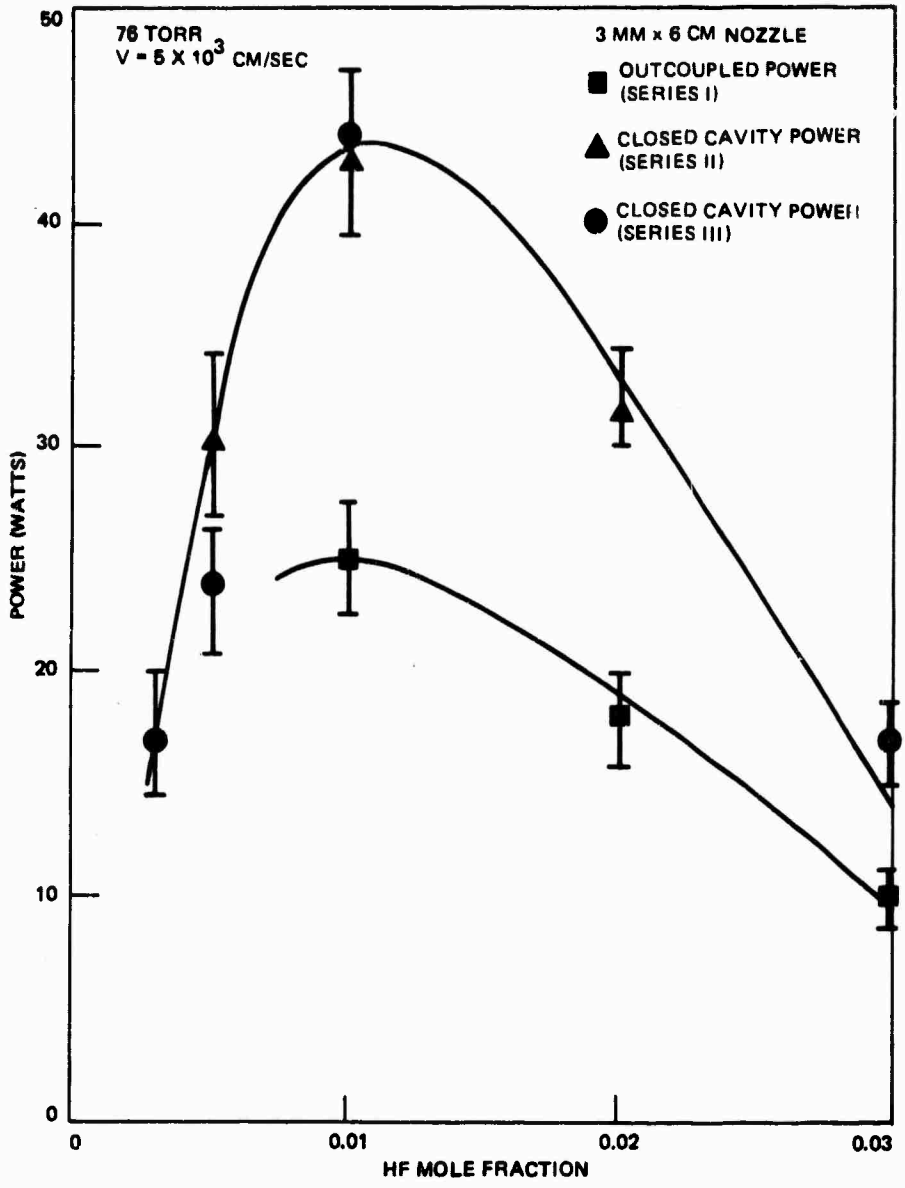

Figure 4. ORTL output power (3 mm x 6 cm nozzle).

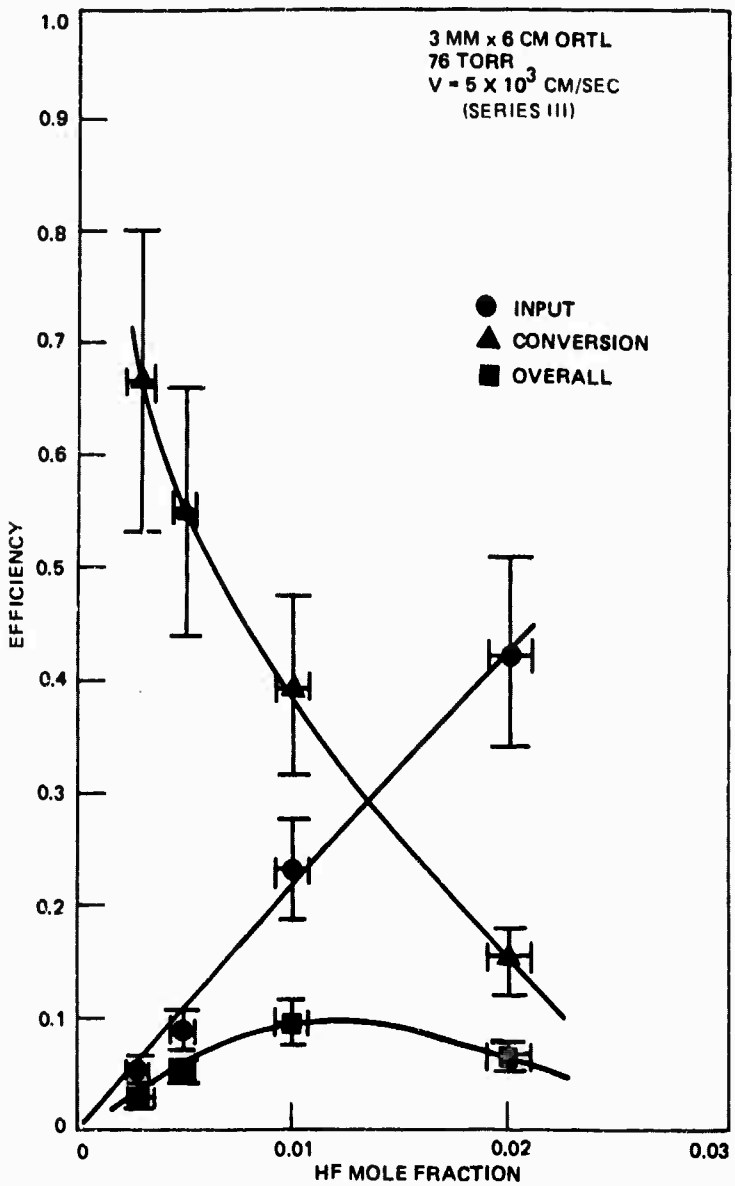

Figure 5. ORTL efficiencies (3 mm x 6 cm nozzle).

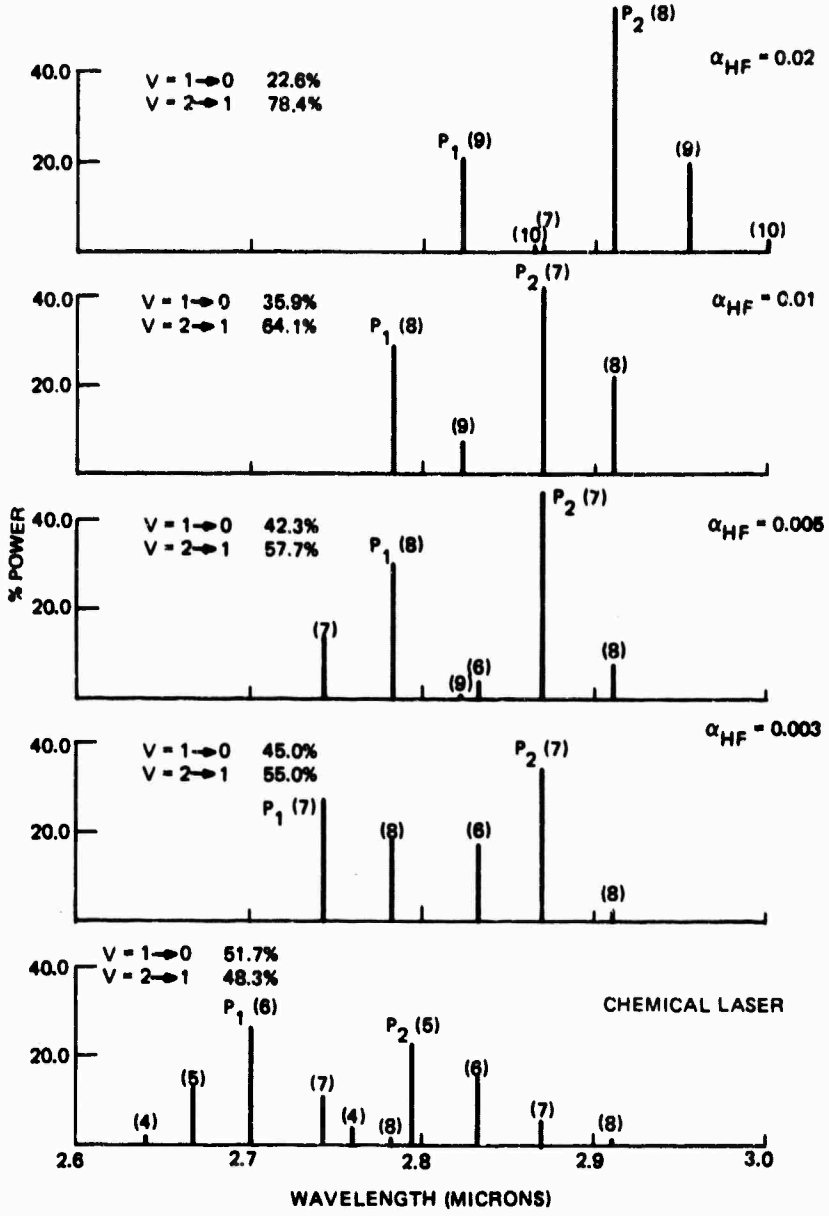

Figure 6. Pump radiation and ORTL output spectra-Series III (3 mm x 6 cm nozzle).

reduced to about 0.12 microns. As the mole fraction of HF increases, so does the gas temperature. Consequently the spectrum shifts to higher J-transitions or longer wavelength. Furthermore, the additional HF also increases the power required to reach the threshold gain required for V=1→0 transitions to oscillate. Therefore the fraction of V=1→0 lasing decreases

with HF mole fraction. The data shows that as HF concentration increased, the balance between the V=1→0 and V=2→1 bands shifted toward the higher vibrational band with as much as 78 percent of the energy being in that band at an HF mole fraction of 2 percent. These results were obtained with no line selection or wavelength sensitive elements in the ORTL resonator.

Results for the 6 mm x 6 cm ORTL cell (Series IV and V) are presented in Figures 7 to 9. The maximum observed power extraction was 52 watts corresponding to an overall efficiency of 12.6 percent. In this cell, the input coupling efficiencies are generally greater than for the previous cell because of the increased absorption path length. However, the conversion efficiencies are reduced. This is a result of the absorbed power at any location being lower than for the 3 mm cell. This situation results from a reduction in the total two-way pump intensity at any point. The increase in input coupling efficiency, reaching a maximum of 66.5 percent, is greater than the loss in conversion efficiency yielding larger overall efficiencies.

The effect of operating pressure on the overall efficiency can be observed by close comparison between Series V and VII, and between Series VIII and IX. With the same pump radiation, overall efficiency appears to be better at higher operating pressure within the 40 to 110 torr range. Unfortunately, this trend is inconclusive because the differences between power values were within experimental uncertainties. In Series V and VIII, where different pump radiation conditions were used, the optimum overall efficiencies were 12 percent, but peaked at 1.0 percent HF in Series V and at 0.5 percent HF in Series VIII. Since the pump radiation in Series VIII had relatively low J-distribution, it had better coupling with the HF molecules in the ORTL medium, and the optimum coupling occurred at lower HF mole fraction in this series.

Results obtained with the 3 mm x 3 cm ORTL cell (Series X) are presented in Figures 10 to 12. The same value of 12 percent overall efficiency was achieved but at higher HF mole fraction, 2 percent. A factor of two increase in pumping intensity resulted in the coupling optimization at higher HF mole fraction. The highest ORTL output per unit volume, 110 watts/cm^3, was achieved here at 76 torr with 1.5 percent HF.

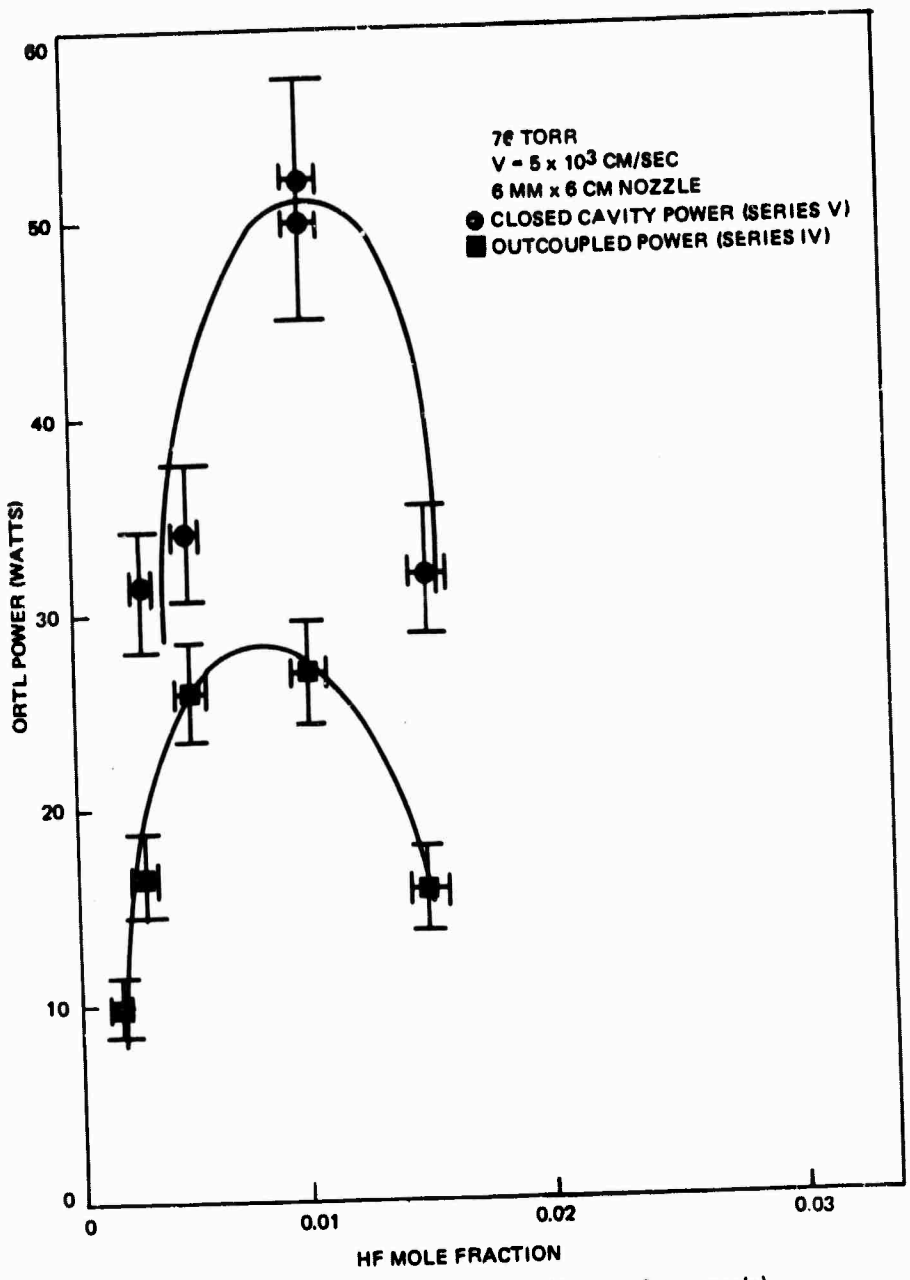

Figure 7. ORTL output power (6 mm x 6 cm nozzle).

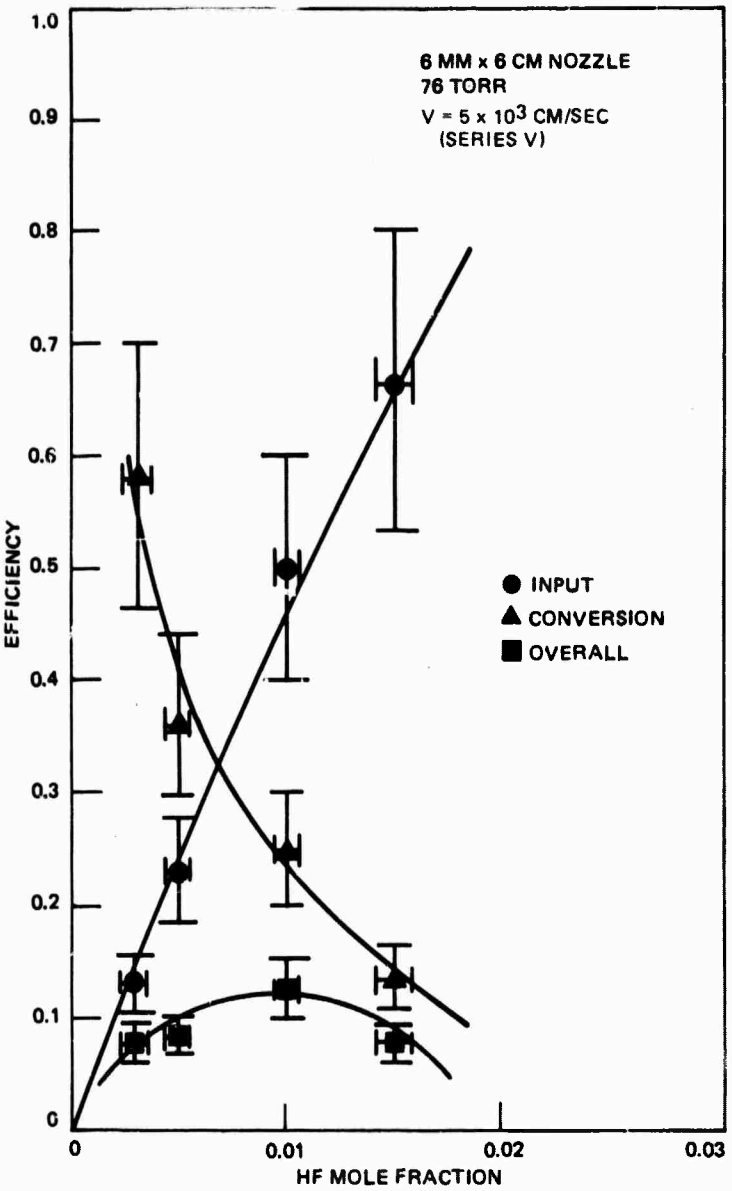

Figure 3. ORTL efficiencies (6 mm x 6 cm nozzle).

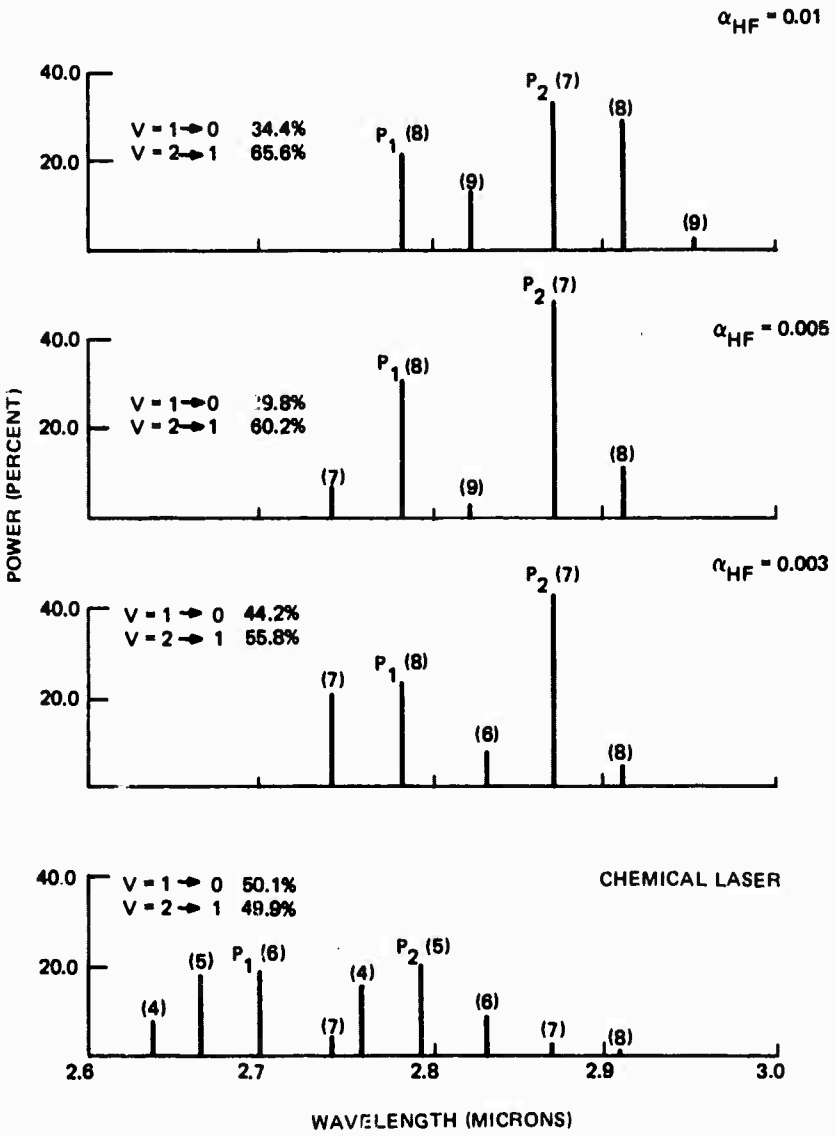

Figure 9. Pump radiation and ORTL output spectra-Series V (6 mm x 6 cm nozzle).

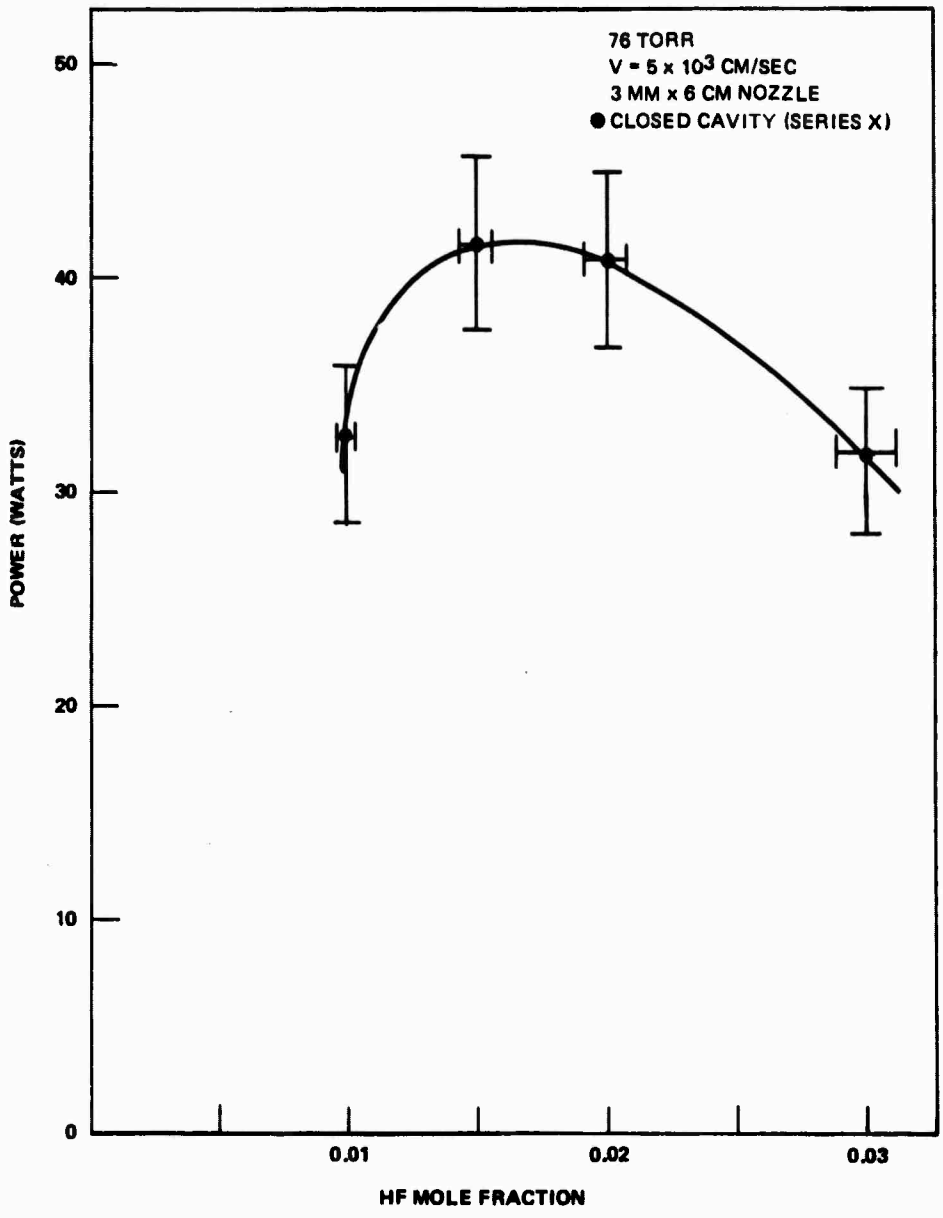

Figure 10. ORTL output power (3 mm x 3 cm nozzle).

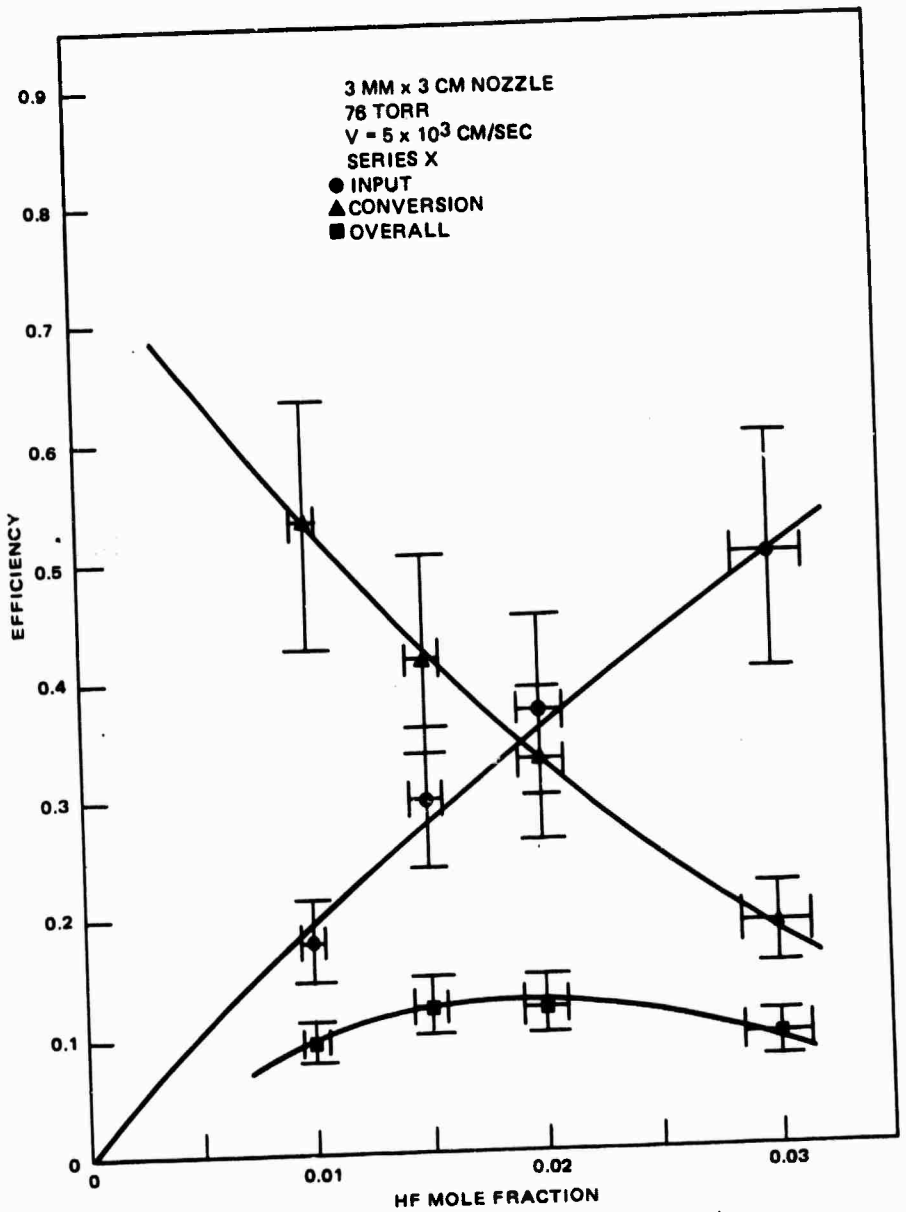

Figure 11. ORTL efficiencies (3 mm x 3 cm nozzle).

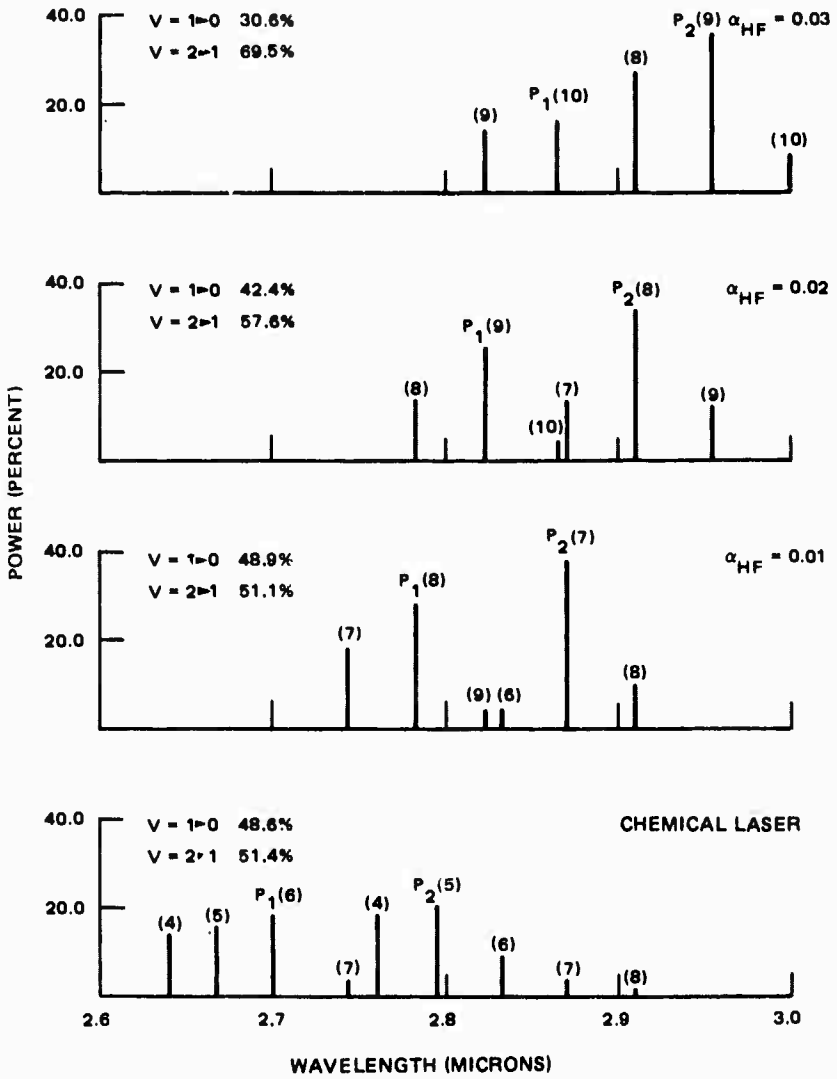

Figure 12. Pump laser and ORTL output spectra-Series X (3 mm x 3 cm nozzle).

In summary, the maximum observed power extraction was 52 watts corresponding to an overall efficiency of 12.6 percent (case V-3). The highest conversion efficiency was 67 percent at 76 torr with 0.3 percent HF (case III-1). The highest ORTL volumetric power was 110 watts/cm^3 at 76 torr with 1.5 percent HF (case X-2). The apparatus utilized was not designed for high efficiency, but was designed to provide a simple versatile ORTL cell for experimental investigation of a number of potential ORTL systems. The issues involved in proper ORTL cell design to achieve maximum overall efficiency are illustrated by these experiments. Optimum conversion efficiency mixtures result in lower input coupling efficiency for a particular geometry. The two can only be maintained at a high level in a larger system operating far above threshold. In order to preserve the high conversion efficiency at low HF concentration and simultaneously achieve high input coupling efficiency, the optical absorption path length has to be increased. In an extra-cavity system design for high overall efficiency, high conversion efficiency would be maintained at a sacrifice in specific input efficiency, but a large absorption path length would be used to achieve high input efficiency. A multiple pass extra-cavity ORTL cell based upon this concept will be discussed in the next section.

2.5 EXTRA-CAVITY MULTIPLE PASS ORTL CELL EXPERIMENTS

The multiple pass cell extracavity configuration represents a laboratory effort at demonstrating efficient overall conversion of pump power to ORTL power. Its design and shape is a radical departure from the previously used rotated ORTL cell which had employed a double pass optical coupling geometry. In the multiple pass design, the pump radiation is trapped between two flat parallel reflectors, causing it to undergo multiple reflections as it pumps the ORTL medium. A photograph of the apparatus is shown in Figure 13. The pump beam enters through the tube at the right and exits the ORTL cell into the cylindrical box at left center. At that point it is either absorbed or reflected back into the ORTL medium. The ORTL resonator optics are mounted in two large rectangular boxes which are shown each with one side removed. The ORTL medium flows vertically upward and is exhausted through the

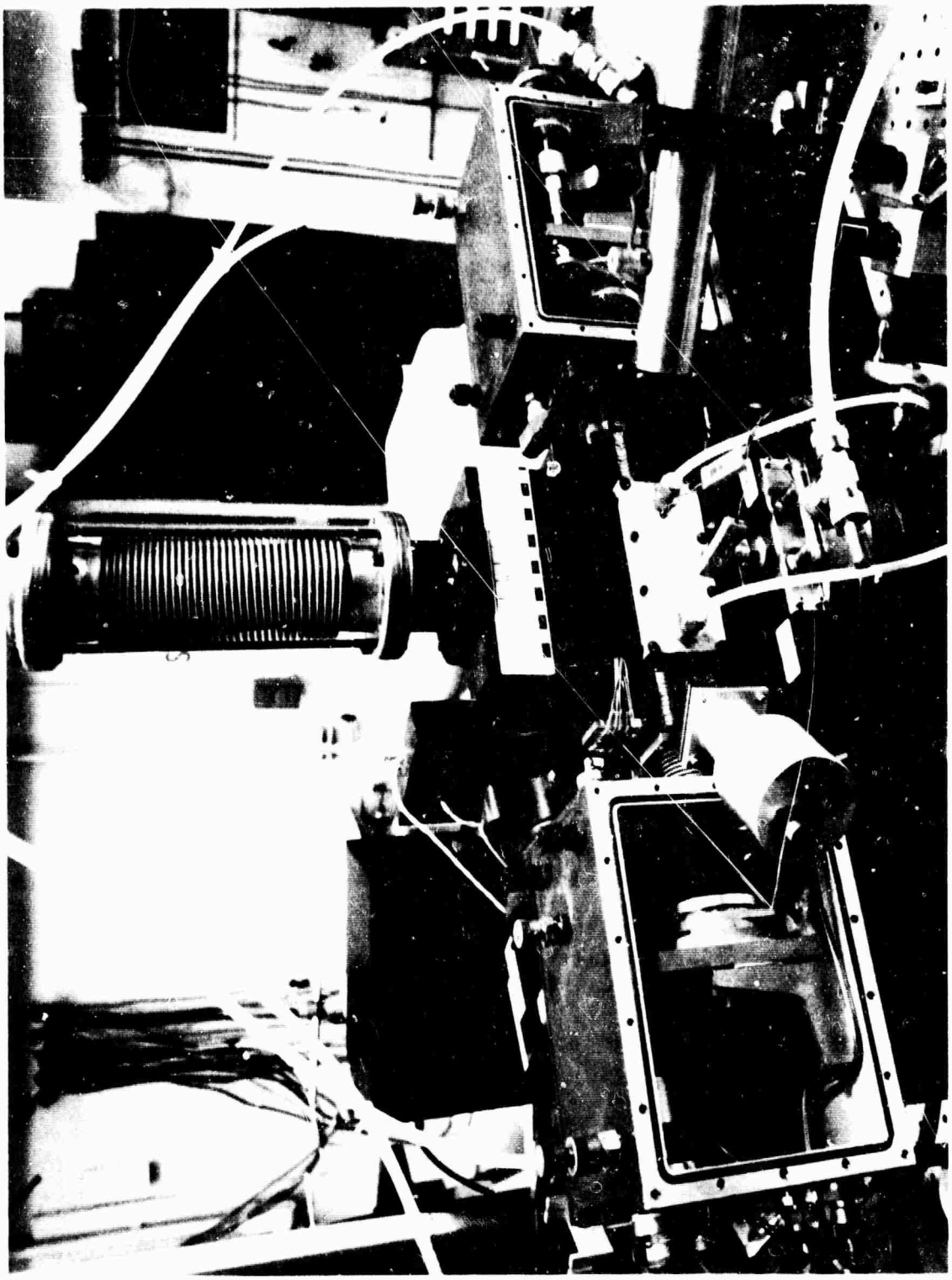

Figure 13. Multiple pass cell experimental configuration.

bellows assembly in the center of photograph. The ORTL gas supply lines and side mirror water cooling lines are also observable in the foreground.

2.5.1 Cell Design and Experimental Configuration

The design of a multiple pass cell for extracavity optical pumping must address three issues: volumetric size, optical walkoff of the pump beam, and gas flow design. If a chemical laser beam of width W is incident on a set of parallel reflectors separated by a distance D at an angle θ, the following geometric relations may be derived assuming that the beam fills the space between the mirrors. Referring to Figure 14, the pump beam width is related to the mirror spacing by

$$W = 2D \sin \theta \tag{1}$$

The number of reflections N_R, in the gain length L is

$$N_R = L/D \tan \theta \tag{2}$$

The absorption path length L_o, through the ORTL medium is given by

$$L_o = L/\sin \theta \tag{3}$$

Coupling of energy into the ORTL cell is most efficient when Equation (1) is satisfied, and the medium is completely covered. Under these conditions, the effective incident pump irradiance is twice the incident irradiance at the cell entrance. If the pump beam width is less than this, then non-uniform pumping results.

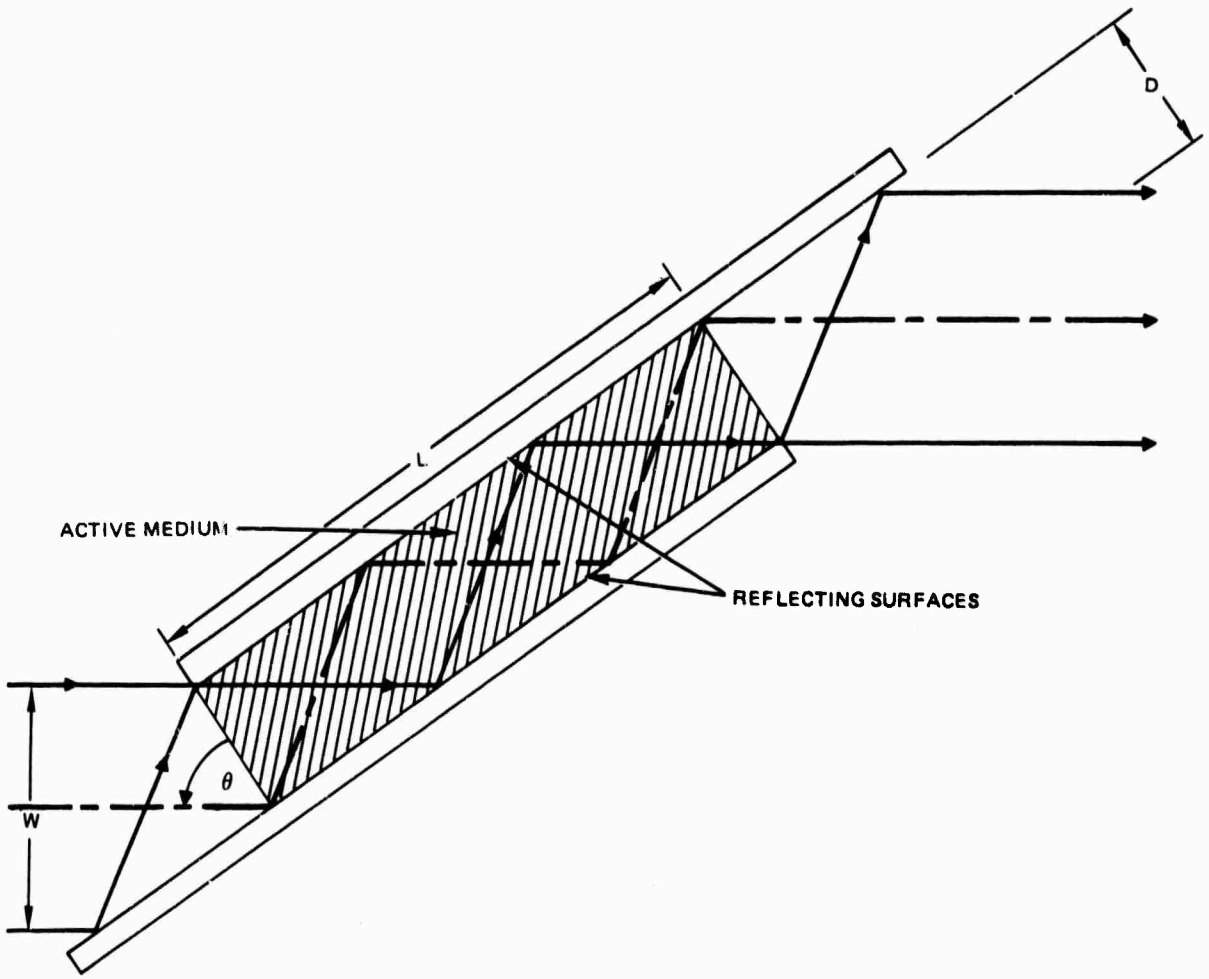

Figure 14. Multiple pass cell geometry.

As the beam propagates down the cell, it experiences reflections off the side mirrors. If the deviation of the mirrors from parallelism is denoted by ϕ, the walk-off h_n, after n bounces is given, for small ϕ, by

$$h_n \cong nD\phi[(n/2) + 1] \tag{4}$$

where n is an even integer.

Utilizing these relationships, design parameters were chosen to be consistent with chemical laser constraints. Choosing $\theta = 45°$, D = 1.1 cm, and $N_R = 8$ gave W = 1.56 cm, L = 8.8 cm, and L_o = 12.4 cm. The actual

implementation was slightly different and is shown in Figure 15. The two water cooled flat aluminum mirror sidewalls were attached directly to the cell body. The cell sides and mirror mounting surfaces were machined parallel to within 5×10^{-4} radians. This tolerance was designed to have less than 3 percent walk-off. The two mirrors were 2.5 cm high. One was 11 cm long and the other 14.3 cm. The additional length beyond the 8.8 cm ORTL gain region accommodated a 1.1 cm region of helium flow at each end in order to confine the ORTL medium and prevent an absorptive region from forming. The pump beam entered at 45 degrees to the side mirrors through a CaF_2 window and underwent eleven reflections before exiting. For some of the experiments, a total reflector was used at the output in order to return the unabsorbed pump radiation and utilize its energy. The chemical laser beam height of 1.6 cm and the ORTL medium flow cross-section defined an excitation volume of approximately 15.5 cm^3.

The multiple pass cell gas plenum contained a rectangular duct which was partitioned into three chambers. Through the middle chamber, 1.1 cm x 8.8 cm cross-section, entered the primary HF/He mixture. At each end a 1.1 cm x 1.1 cm chamber injected helium to confine the primary flow. Fine mesh screens were used to ensure flow uniformity. The ORTL optical axis was located 2.5 cm above the last screen. At that distance the boundary layer thickness in the absence of gas heating was estimated to be 0.8 mm at 76 torr. Plenum pressure and cavity pressure were monitored by pressure transducers. The cavity pressure was set using a 0-100 torr Wallace and Tiernan vacuum gauge.

Heating of the ORTL medium was measured by eight thermocouples located 3.0 cm above the ORTL axis. The thermocouples were located along the 8.8 cm gain length and across the 1.1 cm width with each thermocouple bead located on line center. The thermocouples were spaced 1.1 cm apart starting 0.5 cm from one end. The temperature rise ΔT_A, used to calculate the power absorbed by the gas, was determined by taking an average of the six inner thermocouple readings. Comparison of the temperatures measured along the optical axis provided a measure of energy deposition uniformity. An example of the uniformity observed at various HF concentrations is shown in Figure 16 for the double pass configuration. As expected,

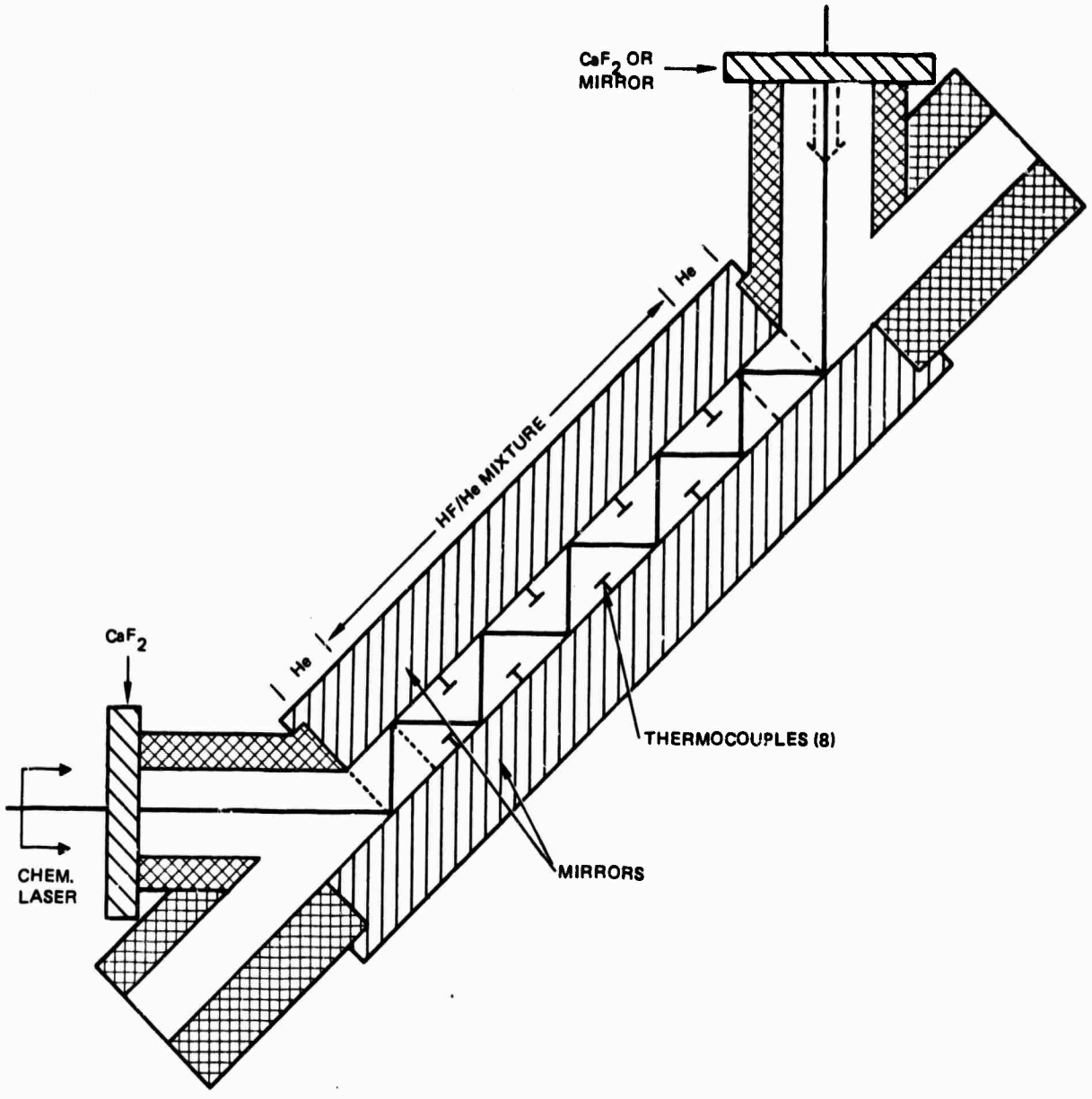

Figure 15. Multiple pass cell schematic.

the decrease in bleaching associated with increasing HF concentration results in non-uniform energy deposition.

A schematic diagram of the overall experimental configuration is shown in Figure 17. The chemical laser output was measured at P_1 by a calibrated 1 kw laser power meter (Coherent Radiation Model 210). The reflection off the CaF_2 window was split at another CaF_2 window as shown. The power meter was usually located at P_2 with the P_1 measurement serving as a calibration. A fast response pyroelectric radiometer (Laser. Precision Model RK-3440) was located at I_o. A second pyroelectric detector at I_1 was used to determine the ratio I_1/I_o. The detectors at I_o and I_1 were individually calibrated by using the Coherent Radiation power meter to measure the power at P_1 and P_3. This data was then used to calibrate the ratio I_1/I_o. The pyroelectric radiometers were then used to measure the throughput of the multiple pass cell with no ORTL medium, and subsequently the ORTL medium absorption or input coupling efficiency. For double pass experiments a total reflector replaced the CaF_2 window at the cell exit.

The ORTL resonator optics consisted of a 3 meter radius concave mirror and a flat mirror separated by 47 cm. These calorimetric closed cavity mirrors were described in the previous section. Outcoupling experiments were not attempted. The side mirrors were coated with Ag/ThF_4. The reflectivity of these mirrors was measured by HF laser calorimetry to be 97.55 ± 0.04 percent indicating water band absorption in the coatings. Unfortunately scheduling considerations did not permit improvement of the reflectivity. These mirrors were water cooled and thermocouples were located at the coolant inlet and exit to monitor the temperature rise. The water flow rate was also measured, thus allowing calculation of the power deposited in the side mirrors.

2.5.2 Cell Characterization Experiments

A series of single pass experiments was conducted in order to characterize the basic cell performance. The following major parameters were included in the measured quantities: pump power incident on the ORTL cell, power deposited in the ORTL medium, extracted ORTL power as deposited in the closed cavity resonator mirrors, pump power absorbed by the side

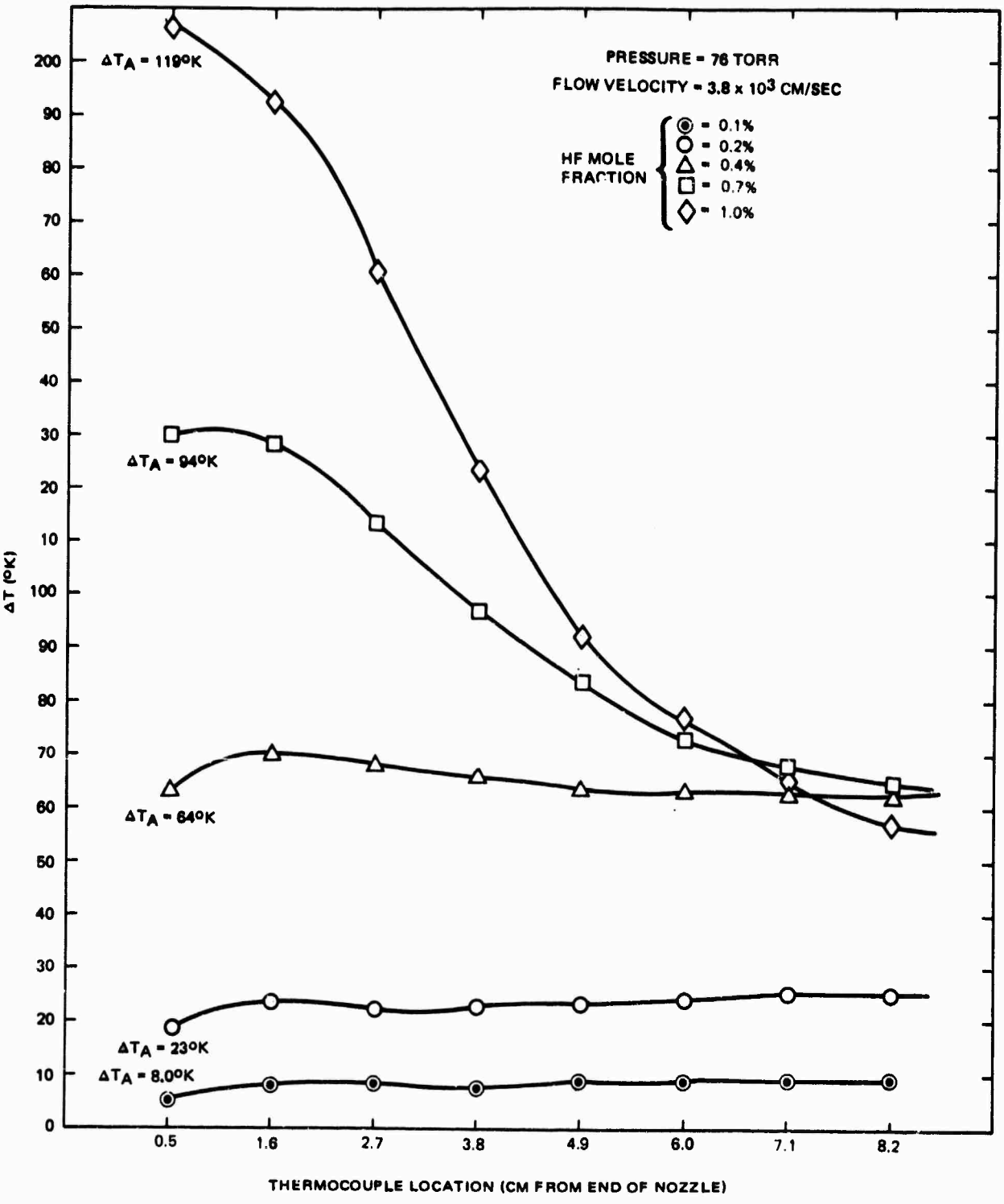

Figure 16. Multiple pass cell gas temperature rise profile.

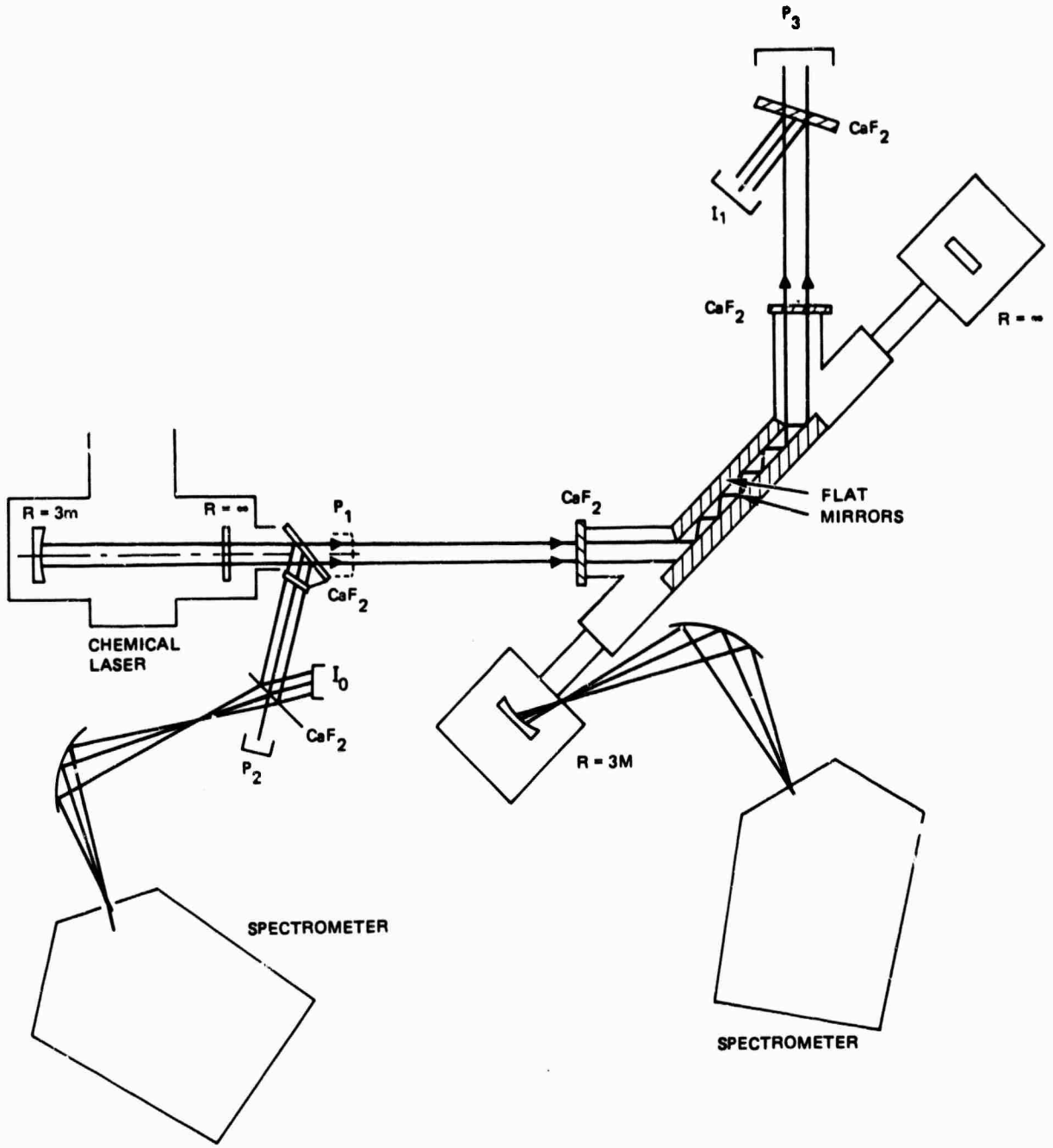

Figure 17. Experimental configuration for multiple pass cell experiments.

wall mirrors, and pump power transmitted through the cell (both with and without HF present). Although these parameters were measured independently by different techniques, the measured values must satisfy a power conservation equation. Consistency checks based upon this equation were used to gain confidence in the measured ORTL performance parameters. This conservation equation will now be discussed.

Referring to the experimental schematic in Figure 17, P_1, the power incident on the cell, passes through three CaF_2 windows and reflects off the side mirrors before it is monitored at P_3. In the absence of HF in the cell

$$P_3 = P_1(0.94)^3(1-M) \tag{5}$$

where 0.94 is the transmission through two surfaces of CaF_2 near normal incidence, and M is the cumulative absorption loss in the side mirrors. With HF in the cell, the power at P_3 is diminished due to the absorption by the gas and the ORTL lasing. Therefore, if the power absorbed by the side mirrors does not change

$$\frac{(P_3 - P_{3g})}{(0.94)^2} = \dot{Q} + P_{ORTL} \tag{6}$$

where P_{3g} is the power measured with HF present in the cell, $\dot{Q}$ is the power deposited in the gas, and P_{ORTL} is the ORTL laser power. Combining Equations (5) and (6), one obtains

$$0.94\,P_1 = P_M + P_{ORTL} + \dot{Q} + P_{3g}/(0.94)^2 \tag{7}$$

where $P_m = 0.94\,P_1\,M$ is the power absorbed by the side mirrors. Equation (7) represents the power balance in the multiple pass cell, and serves as the power conservation equation for data consistency checks.

The input coupling efficiency can be obtained from P_{3g}/P_3, as well as from the pyroelectric radiometer signals with and without HF in the ORTL cell, inasmuch as

$$\frac{P_{3g}}{P_3} = \frac{R_g}{R} = 1 - \eta_I \qquad (8)$$

where $R_g = I_1/I_o$ with HF in the ORTL cell, and $R = I_1/I_o$ without HF in the cell.

Table 3 summarizes the single pass results. The pressure and velocity were fixed at 76 torr and 3.8×10^3 cm/sec respectively and the HF mole fraction was varied from 0.1 to 1.0 percent. The input pump power P_1, exit pump powers P_3 and P_{3g}, extracted ORTL power P_{ORTL}, and the power absorbed by the gas $\dot{Q}_2$ are listed in columns 2 through 6. The estimated uncertainty for these quantities is 5 percent. The exit pump power difference when corrected for CaF_2 transmission as indicated in Equation (6) should equal $\dot{Q} + P_{ORTL}$. Comparison of columns 7 and 8 indicates agreement to within the experimental uncertainties.

The side mirror absorption M, in the absence of HF obtained from P_1 and P_3 using Equation (5) is tabulated in column 9. The power absorption in the side mirrors, $P_M = 0.94\ P_1 M$, is listed in column 10. In columns 11 and 12, the values calculated from Equation (7) in the presence of HF are listed. The estimated uncertainty for P_M is 10 percent. Evidently, (from columns 10 and 11) the side mirror absorption was unchanged when HF was present in the cell.

There are two contributions to the power absorbed by the side mirrors: the absorption due to the irradiance incident on the mirror surfaces and the heat transfer from the ORTL medium to the side mirrors. When HF was added to the ORTL medium, the pumping power incident on the side mirrors decreased; hence the first contribution decreased. On the other hand, the temperature of the ORTL medium increased, and consequently the second contribution increased. The nearly constant power absorbed by the side mirrors with and without HF present may possibly be due to a balance of these two contributions.

The average value of M is 31 ±1 percent. The corresponding single surface reflectivity is 96.8 ±0.4 percent. The value of M could be reduced to 4.4 percent by the use of dielectric coatings. This would increase the incident power utilization. To eliminate this factor from ORTL performance

TABLE 3. SUMMARY OF SINGLE PASS RESULTS WITH MULTIPLE PASS ORTL CELL

1	2	3	4	5	6	7	8	9	10	11	12	13	14	15
HF (%)	P_1 (watts)	P_3 (watts)	P_{3g} (watts)	P_{ORTL} (watts)	$\dot{Q}$ (watts)	$(P_3 - P_{3g})/0.88$ (watts)	$\dot{Q} + P_{ORTL}$ (watts)	M (%)	P_M (watts)	P_M (watts)	M (%)	P_{3g}/P_3	R_g/R	$1 - \eta_I$
0.1	893	522	480	18.8	27.5	48	46.3	29.6	250	250	29.8	0.93	0.90	0.92
0.2	955	555	417	50.0	46.3	122	96.3	30.0	269	296	33.0	0.81	0.84	0.84
0.4	959	563	369	59.1	139	220	198	29.3	264	285	31.7	0.66	0.68	0.68
0.7	1029	602	255	55.3	319	392	374	29.6	286	305	31.4	0.42	0.43	0.43
1.0	1034	605	192	14.8	425	467	440	29.6	289	315	32.4	0.32	0.34	0.33

evaluation, the 31 percent power loss to the side mirrors was taken into account in the computation of the input efficiency in Table 3 as follows:

$$\eta_I = \frac{\dot{Q} + P_{ORTL}}{0.94\, P_1 - P_M} \tag{9}$$

where $0.94\, P_1$ is the power transmitted through a CaF_2 window into the ORTL cell. Columns 13 and 14 list the transmission through the cell for different mole fractions of HF.

The agreement between the two columns is better than the estimated uncertainty of ±5 percent. Column 15, $1 - \eta_I$, is obtained from columns 2, 8, 11 and Equation (9). The agreement of column 15 with the two previous columns is significantly better than the expected uncertainty of 25 percent for η_I estimated from the experimental data using Equation (9). This comparison serves as a check for the different instrumentation used to measure each of the parameters need to calculate η_I.

A second group of experiments was performed to obtain a direct comparison between single pass and double pass performance under otherwise identical experimental conditions. Of interest was the change, not the absolute values of the efficiencies.

The ORTL pressure and velocity were chosen to be 76 torr and 3.8×10^3 cm/sec respectively, corresponding to a flow rate of 150 millimoles/sec. The experimental configuration was the same as in Figure 17, but for double pass operation a flat mirror replaced the CaF_2 exit window on the cell. The average pump power incident on the ORTL cell was approximately 1 kw and was distributed among P(4) to P(7) transitions in the V = 2→1 and V = 1→0 vibrational bands. (This is the same as in the previous set of single pass experiments.) The irradiance incident on the ORTL cell was approximately 350 W/cm^2. The ORTL power and the calculated efficiencies are listed in Table 4. The upper and lower entries in each box are the single pass and double pass values respectively. The overall efficiency, η_T, is defined by taking into account the power loss into the side mirrors in a manner similar to that used for η_I

$$\eta_T = \frac{P_{ORTL}}{0.94\, P_1 - P_M} \tag{10}$$

The conversion efficiency, η_c, is given by

$$\eta_c = \frac{P_{ORTL}}{P_{ORTL} + \dot{Q}} \tag{11}$$

Equations (9) and (11) were applied to both single and double pass experiments. As stated previously, the estimated uncertainty for P_1, P_{ORTL}, and $\dot{Q}$ is 5 percent and for P_M is 10 percent. The resultant uncertainties for η_I, η_c, and η_T are 25, 15 and 20 percent respectively.

In double pass experiments, I/I_o and transmitted power could not be measured. P_M was measured directly from the temperature rise in the side mirror cooling water. An average value of 32 ±2 percent was determined for M using P_1 and P_M data listed in Table 4. The fact that the single and

TABLE 4. SINGLE PASS/DOUBLE PASS COMPARISON

α_{HF} (percent)	P_1 (watts)	P_M (watts)	$\dot{Q}$ (watts)	P_{ORTL} (watts)	η_I (percent)	η_c (percent)	η_T (percent)
0.1	893 1051	257 339	18.8 22.8	27.5 42.1	7.9 10.0	59.0 64.9	4.7 6.5
0.2	955 1068	292 344	50.0 63.7	46.3 72.9	15.8 20.7	48.1 53.4	7.6 11.1
0.4	959 1068	281 344	139 161	59.0 98.9	31.9 39.3	29.8 38.1	9.5 15.0
0.7	1029 1048	306 337	319 353	55.0 79.0	56.6 66.7	15.0 18.3	8.5 12.2
1.0	1034 1048	311 337	425 474	14.8 43.0	66.5 79.8	3.4 8.3	2.3 6.6

double pass losses were nearly the same even though for the latter geometry the pump beam made twice as many reflections, indicated a possible systematic underestimation of P_M. Cooling of the side mirrors by conduction to the cell structural walls could systematically reduce the cooling water temperature. If P_M is really larger, the values for η_I and η_c are underestimates.

The higher double pass efficiencies demonstrate the increase in ORTL performance with increased chemical laser irradiance. A measure of the additional irradiance available for double pass excitation is given by $1 - \eta_I$ (single pass). For α_{HF} = 0.4 percent a 67 percent increase in ORTL power was observed when 68 percent of the incident power was reflected back into the cell. However Q increased by only 16 percent, indicating a net improvement of conversion efficiency as well as overall efficiency with the increased irradiance. Similar effects are seen at 0.7 percent HF. For α_{HF} lower than 0.4 percent a small percentage improvement in the ORTL power was observed, even though a larger fraction of the pump was returned to the cell. The less than efficient utilization of pump power could be attributed to the insufficient number density of HF present in the medium. Quite the opposite effect was observed for α_{HF} = 1.0 percent. Here the additional 33 percent pump power resulted in nearly a factor of three increase in ORTL power. In this case the ORTL was closer to threshold and consequently was strongly dependent upon effective pump irradiance. The HF mole fraction must be carefully matched to the optical pump power available for excitation.

2.5.3 Efficiency Demonstration Experiments

The objective of this test series was to demonstrate high overall efficiency. Therefore the pump laser power and spectral distribution were optimized here, in contrast to the experiments of the previous section. Chemical laser flow rates were varied to obtain not necessarily the highest overall power, but the highest power with the lowest rotational line distribution. (See the figure of merit discussion in the Mid-Term Technical Report.) The nominal operating conditions arrived at for these experiments are shown in Table 5. The irradiance at the ORTL cell was 250 ±16 watts/cm^2.

TABLE 5. CHEMICAL LASER OPERATING CONDITIONS

Incident Power:	762 ±46 watts		
Beam Shape:	1.75 cm x 1.64 cm ($2.87\ cm^2$)		
Spectral Distribution			
V = 1 → V = 0		V = 2 → V = 1	
Transition	Power (%)	Transition	Power (%)
P(3)	0.1	P(3)	0.9
P(4)	9.5	P(4)	15.7
P(5)	15.9	P(5)	20.1
P(6)	18.2	P(6)	9.9
P(7)	5.2	P(7)	3.7
		P(8)	1.0
	48.7		51.8

Under these conditions a number of experiments were conducted in the double pass configuration. The experimental parameters and measured efficiencies are shown in Table 6. During each experiment the power incident on the ORTL cell P_1, was monitored via the beam splitter arrangement shown in Figure 17, and P_M, the power absorbed by the side mirrors, was monitored as described earlier. The major difference between these experiments and previous ones was the effectiveness of the pump radiation. The ORTL parameters varied were: pressure, velocity, and HF mole fraction.

TABLE 6. EFFICIENCY DEMONSTRATION EXPERIMENTS

Test	Experiment Conditions				Average ΔT (^{o}K)	$\dot{Q}$ (watts)	P_M (watts)	P_{ORTL} (watts)	η_I (%)	η_c (%)	η_T (%)
	HF Mole Fraction (%)	Pressure (torr)	Velocity (10^3 cm/sec)	P_l (watts)							
1	0.1	76	3.8	827	8.0	26.2	264	71.0	18.9	73.1	13.8
2	0.2	76	3.8	799	23.0	73.5	265	110	37.8	60.0	22.7
3	0.4	76	3.8	799	64.0	207	262	121	67.1	36.9	24.8
4	0.7	76	3.8	709	94.2	297	212	74.2	81.8	20.0	16.3
5	1.0	76	3.8	778	119	375	232	38.1	82.9	9.2	7.6
6	0.1	110	3.8	749	8.4	38.1	243	102	30.6	72.9	22.3
7	0.15	110	3.8	714	16.3	74.4	231	121	42.6	61.9	26.4
8	0.2	110	3.8	762	25.2	115	234	133	49.3	53.8	26.5
9	0.3	110	3.8	771	42.9	197	235	116	62.6	37.0	23.2
10	0.4	110	3.8	769	57.5	262	235	78.8	68.2	23.1	15.8
11	0.2	76	1.3	718	62.0	66.8	229	113	40.3	62.9	25.4
12	0.3	76	1.3	758	99.7	107	240	132	50.7	55.2	28.0
13	0.4	76	1.3	764	136	147	239	128	57.4	46.6	26.7
14	0.5	76	1.3	764	165	177	247	128	64.7	41.8	27.1
15	0.7	76	1.3	766	210	226	246	89.3	66.5	28.3	18.8
16	0.3	76	0.65	766	132	71.2	246	124	41.2	63.5	26.1
17	0.4	76	0.65	747	178	95.8	232	135	49.0	58.5	28.7
18	0.6	76	0.65	766	221	119	246	126	51.8	51.4	26.6
19	0.4	76	5.1	773	37	156	259	119	59.0	43.3	25.6

Figure 18 shows the efficiencies obtained as a function of HF mole fraction at 76 torr and 3.8×10^3 cm/sec flow velocity. The one percent HF results are omitted but the high 83 percent input efficiency should be noted. Figure 19 shows similar data at 110 torr. A shift of the peak efficiency to lower HF mole fraction and an increase in ORTL output power from 121 watts to 133 watts were observed at the higher operating pressure. A maximum conversion efficiency of 73 percent was obtained with 0.1 mole percent of HF in each case. The highest ORTL power,

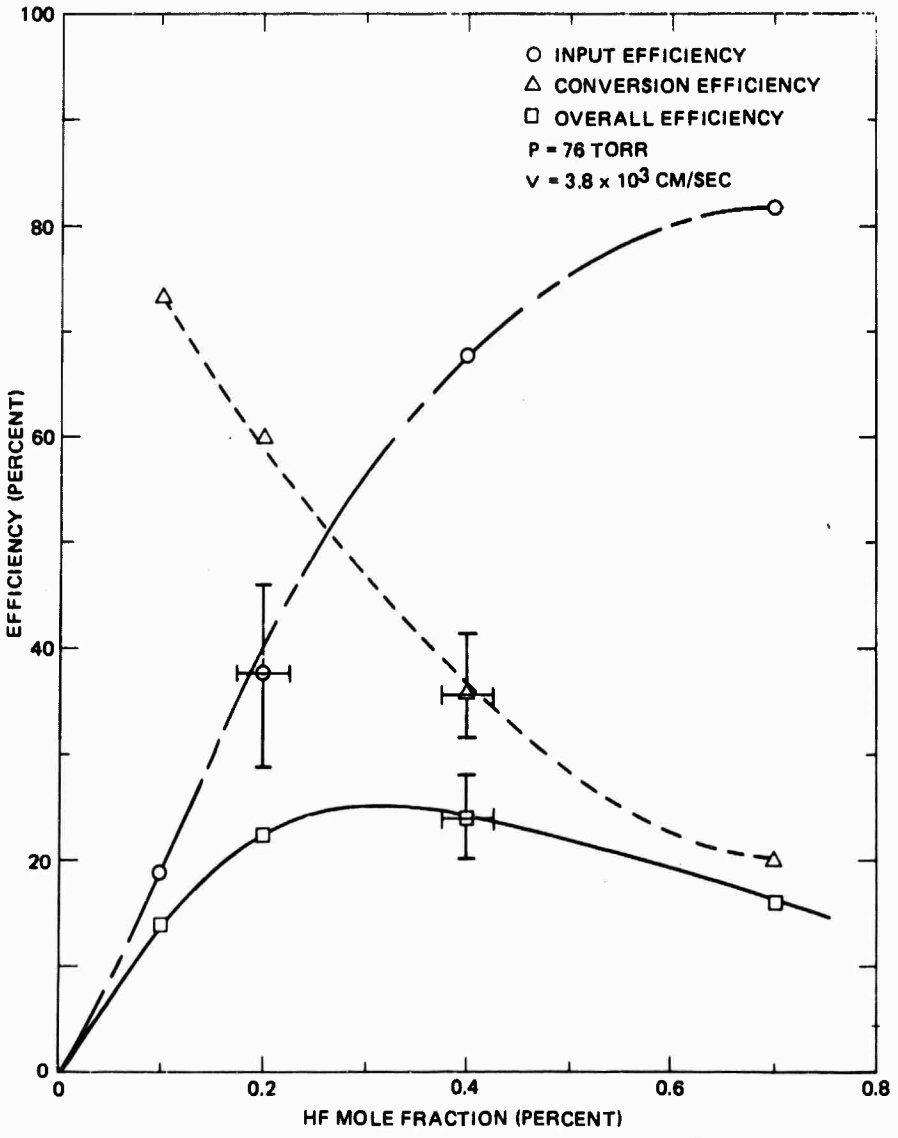

Figure 18. Multiple pass cell efficiencies (76 torr, 3.8×10^3 cm/sec).

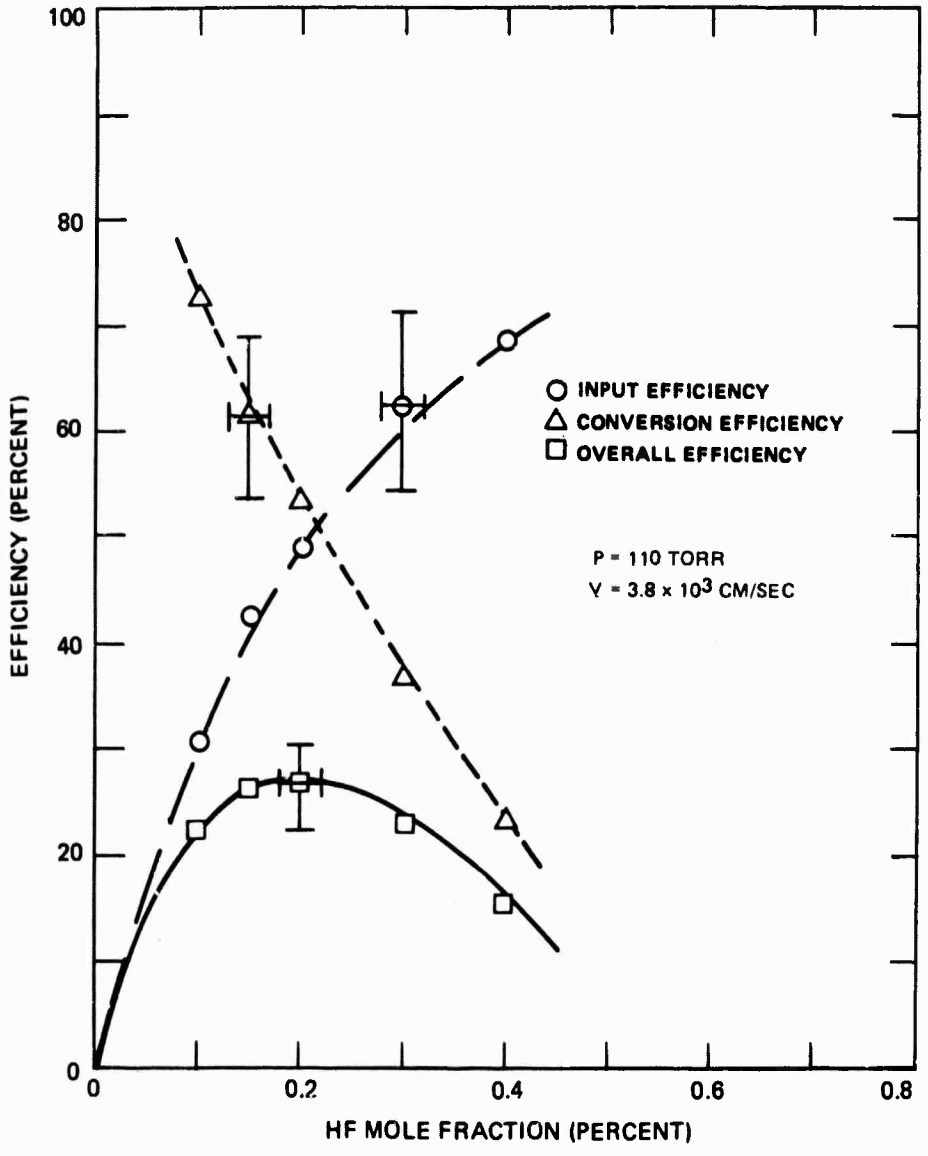

Figure 19. Multiple pass cell efficiencies (110 torr, 3.8 x 10^3 cm/sec).

133 watts, was obtained at 0.2 mole percent at 110 torr; the associated overall efficiency was 27 percent. As the data at both pressures show, for a fixed pump intensity, input coupling efficiency can be increased by increasing the HF mole fraction but there is a sacrifice in conversion efficiency.

Results obtained at 76 torr but at lower gas velocities, 1.3×10^3 cm/sec and 6.5×10^2 cm/sec, are shown in Figures 20 and 21. The maximum observed closed cavity power was 135 watts at a velocity of 6.5×10^2 cm/sec. The side mirrors absorbed 232 watts, leaving 471 watts available to excite the gas. Thus the 135 watts extracted corresponded to an overall efficiency of 29 percent, a conversion efficiency of 59 percent, and an input efficiency of 49 percent.

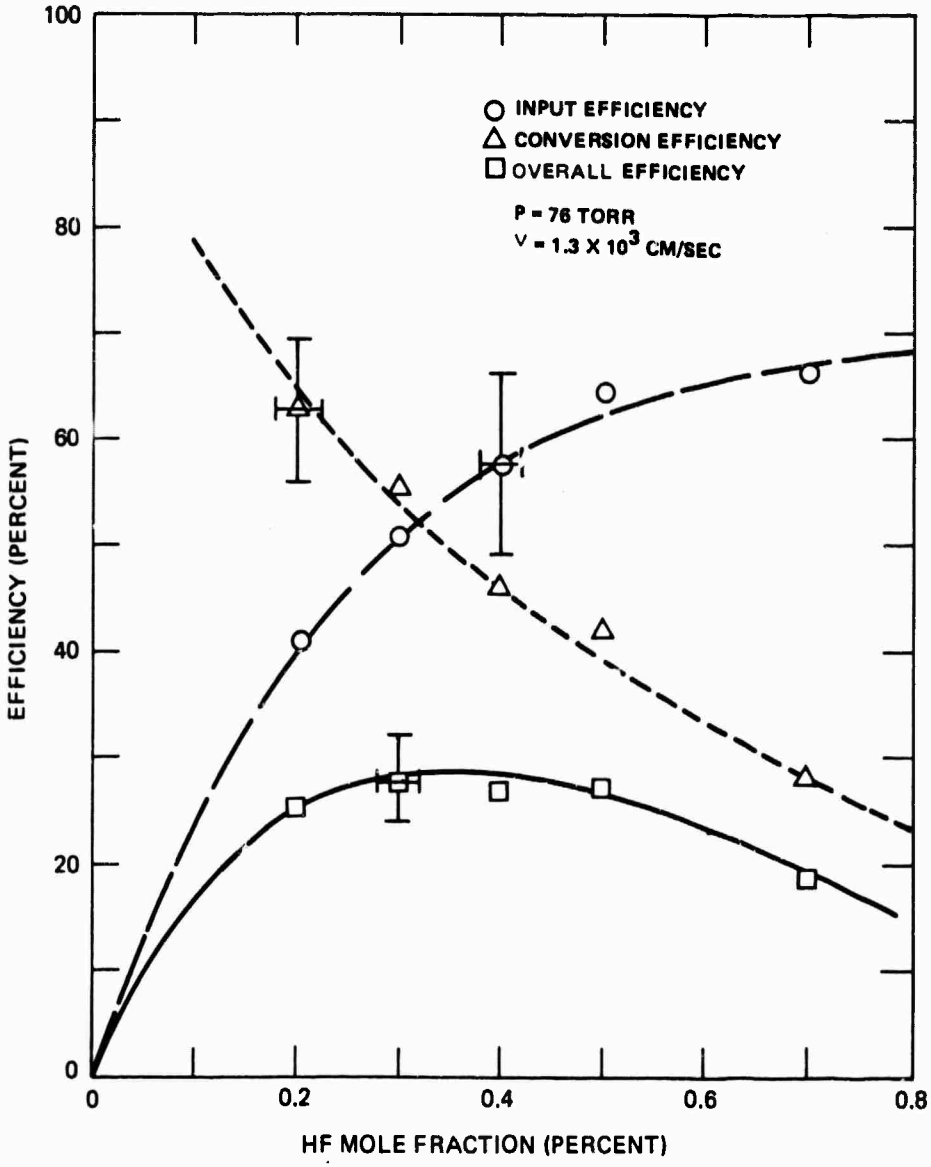

Figure 20. Multiple pass cell efficiencies (76 torr, 1.3×10^3 cm/sec).

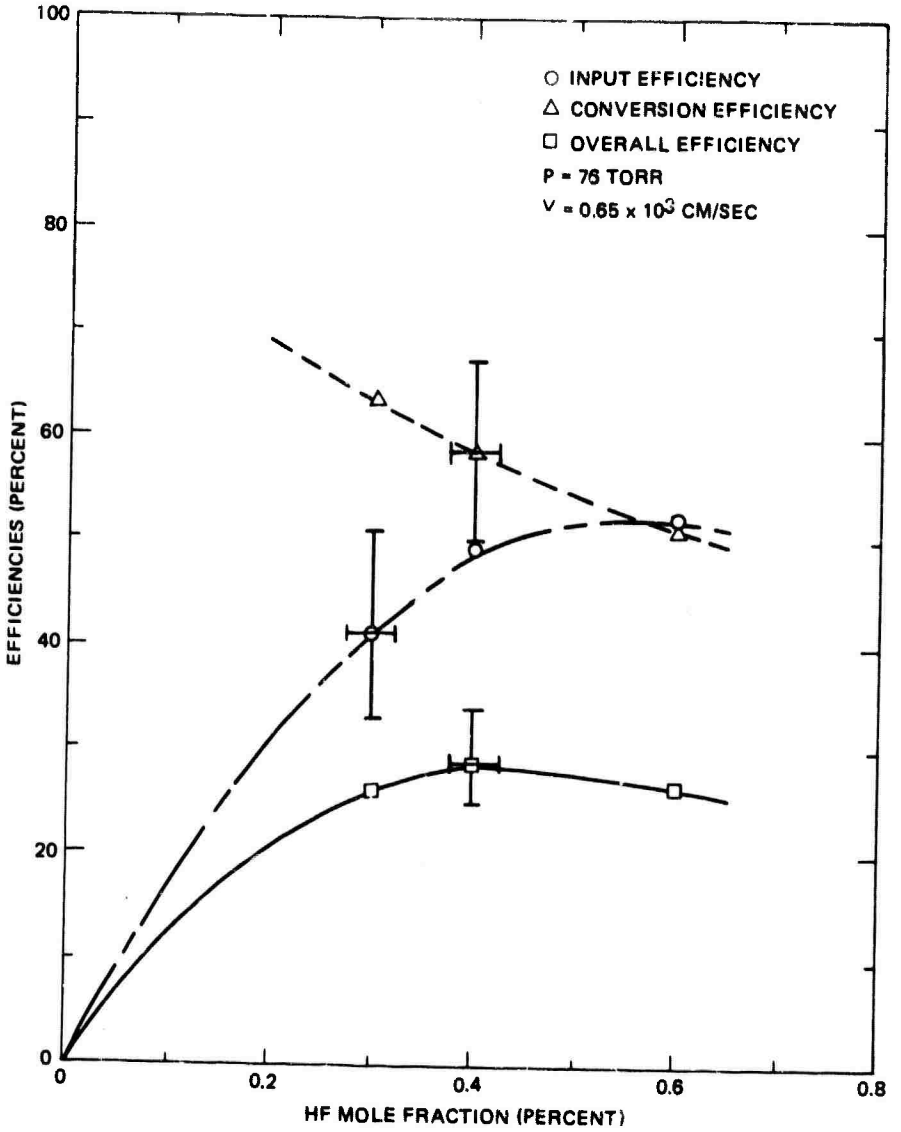

Figure 21. Multiple pass cell efficiencies (76 torr, 0.65 x 10^3 cm/sec).

During each closed cavity power extraction measurement, line spectra of the pump and ORTL outputs were recorded. Representative spectra at 76 torr at two velocities, 3.8 x 10^3 cm/sec and 6.5 x 10^2 cm/sec, are shown in Figures 22 and 23.

The dependence of the overall efficiency on mole fraction, pressure, and velocity can be unified if one realizes that the key parameter is the HF number density. The number density is independent of velocity; it

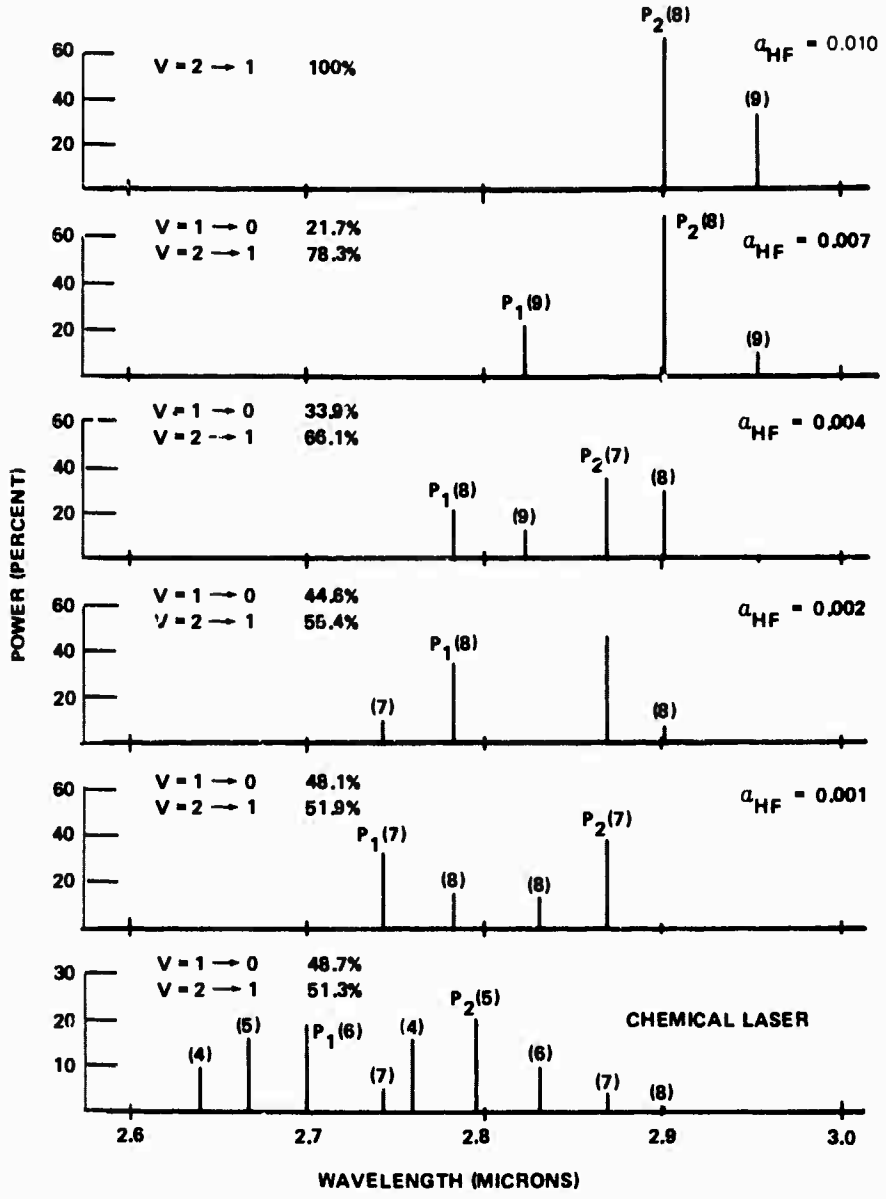

Figure 22. Multiple pass cell output spectra (76 torr, 3.8×10^3 cm/sec).

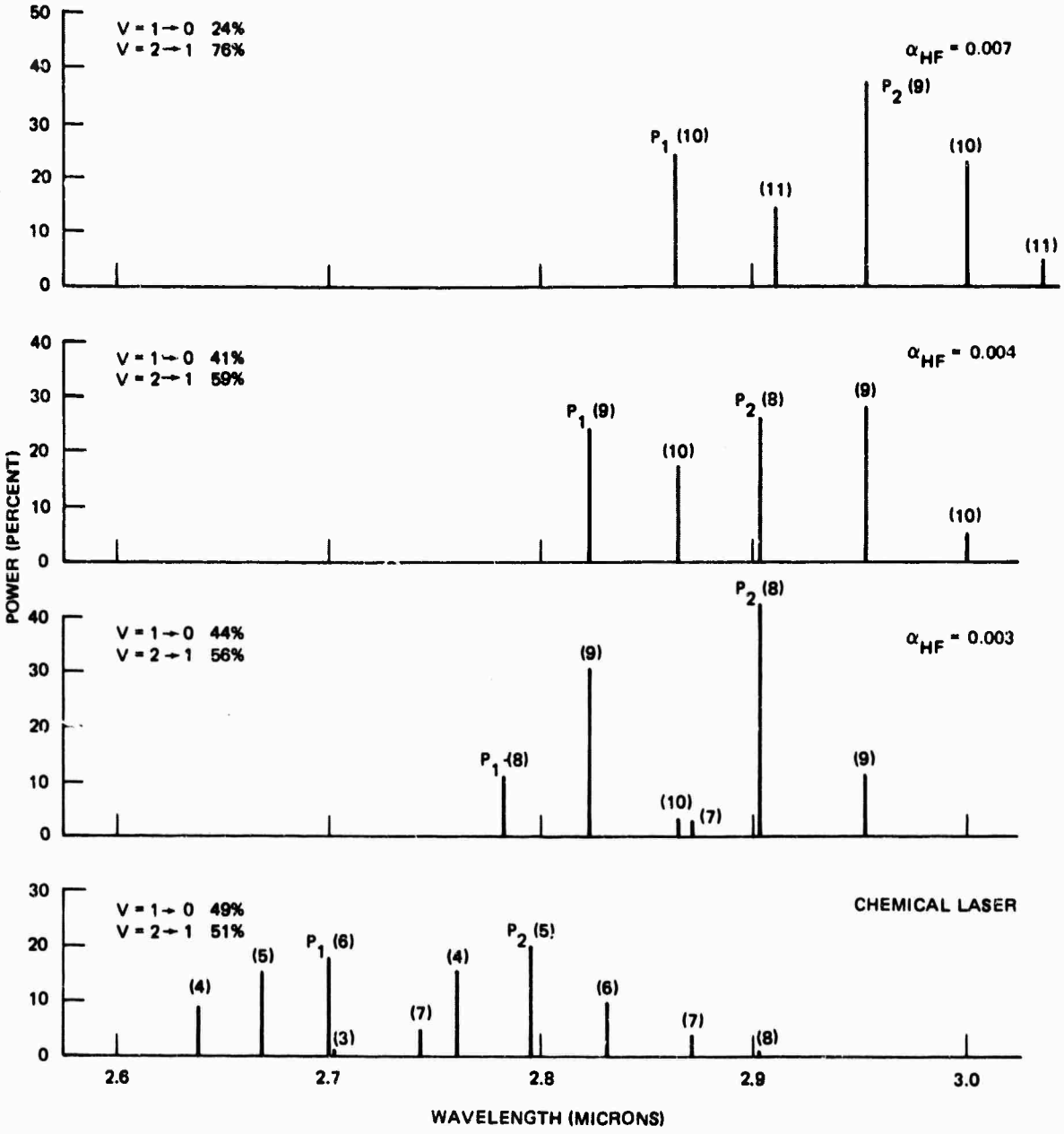

Figure 23. Multiple cell output spectra (76 torr, 0.65 x 10^3 cm/sec).

depends only on the HF mole fraction and total pressure. At 76 torr, for each velocity listed in Table 6, the overall efficiency is a maximum at a mole fraction between 0.4 and 0.3 percent. The number density at 110 torr with α_{HF} equal to 0.2 percent, where the peak overall efficiency is observed, is approximately equal to the value at 76 torr.

The dependence of the overall efficiency on temperature is illustrated in Table 6 by the data taken at 76 torr and α_{HF} = 0.4 percent, Tests 17, 1[illegible] and 3. If one orders the tests according to decreasing $\Delta T_{average}$, the following values are obtained for η_T: 28.7, 26.7, and 24.8 percent. Although the values show a positive correlation with temperature, the range is within the estimated uncertainty for η_T thus the trend is inconclusive. Listing the ORTL power according to decreasing $\Delta T_{average}$ one obtains: 135, 128, and 121 watts. Within the temperature range examined, the ORTL power does increase with temperature. The reason for this trend is the better spectral match between the driving laser and the absorbing gas at the higher temperature.

The pump laser itself of course affects the overall efficiency in a major way. One need only compare the data at 76 torr and 3.8×10^3 cm/sec in Table 6 with that in Table 4 to see that this is so. Higher intensity (350 W/cm^2 versus 250 W/cm^2) in fact yielded a lower overall efficiency (16 percent versus 29 percent). The lower intensity (Table 6) had a greater share of the power distributed among lower P-branch lines. In general, the optimum pump laser spectral distribution is determined by the ORTL gas temperature. In the present experiments the latter quantity could not be varied and so the pump laser distribution was matched to the ORTL medium. Alternatively, the ORTL temperature could be matched to a maximally efficient chemical laser. For a given pump radiation, the average temperature of the ORTL medium can be controlled by varying the inlet gas temperature and velocity and by varying the HF number density. In an optimized ORTL system design the ORTL temperature and the pump laser characteristics could both be optimized together.

Highlights of the extracavity characterization experiments included the following:

Rotated ORTL Cell

1. Maximum power extraction of 52 watts
2. Maximum overall efficiency of 13%
3. Maximum conversion efficiency of 67%
4. Maximum input coupling efficiency of 78%
5. Highest ORTL volumetric power density of 110 watts/cm^3

Multiple Pass Cell

1. Maximum power extraction of 135 watts
2. Maximum overall efficiency of 29%
3. Maximum conversion efficiency of 73%
4. Maximum input coupling efficiency of 83%

3.0 CHEMICAL LASER/ORTL DYNAMICS

When the ORTL cell is placed inside the chemical laser resonator (intracavity configuration), the pump radiation is trapped in the resonator until it is absorbed by either the ORTL medium or the resonator mirrors. When the ORTL medium absorption is much greater than the mirror absorption, one anticipates high input and conversion efficiences, and thus high overall efficiency. However, this configuration presents several complications. Because each pump laser line sees a different load, the lasing spectrum will be different than with usual resonators and will be sensitive to the ORTL conditions. The competition of stimulated emission in the chemical laser resonator and in the ORTL resonator also needs to be dealt with. Finally, the close coupling between the pump laser and ORTL may cause dynamic effects.

The primary objective of this task was the characterization of the temporal behavior of the chemical laser and ORTL outputs. No emphasis was placed on efficient operation of this configuration. The rotated ORTL cell designed for extracavity use was modified for intracavity use, and a CaF_2 Brewster window was used to separate the ORTL and the chemical laser media. The selected chemical laser resonator was a simple stable resonator. Since there is no feedback interaction in the extracavity configuration, results in that configuration were used as a baseline for comparison.

Schematic diagrams for intra- and extra-cavity configurations are shown in Figures 24 and 25. The extracavity configuration was identical to that used in the experiments described in section 2.4. In the intracavity experiments both an orthogonal 3mm x 3cm cell and a rotated 3mm x 6cm at an angle of 20 degrees, were used. The pump laser resonator consisted of a 3 meter radius concave mirror and a flat mirror, separated by 90 cm when the orthogonal ORTL cell was used and by 120 cm with the rotated cell. The ORTL resonator consisted of a 3 meter radius total reflector and a 1.9 percent transmitting flat outcoupler.

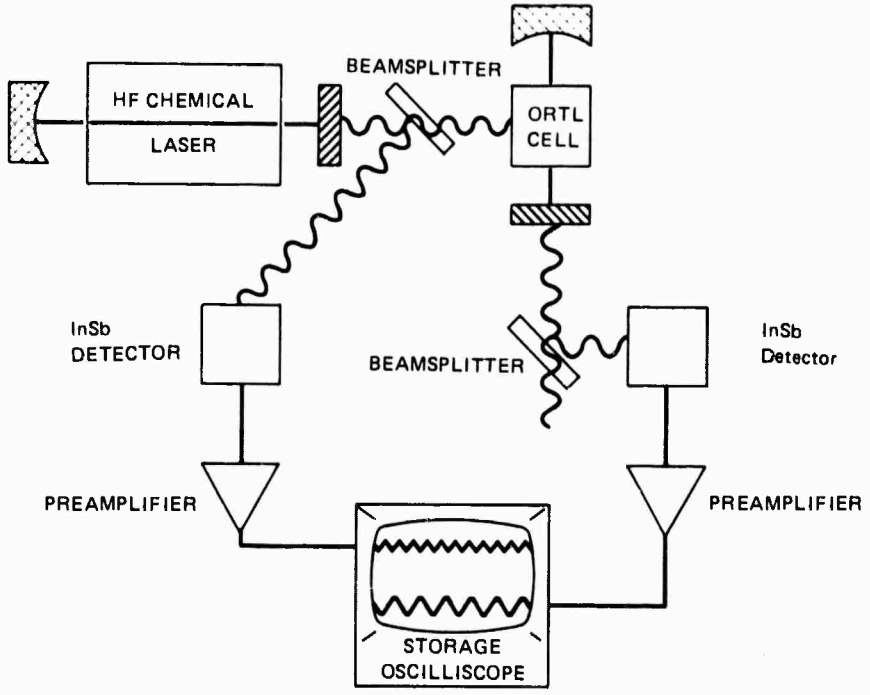

Figure 24. Extracavity configuration for chemical laser/ORTL dynamics study.

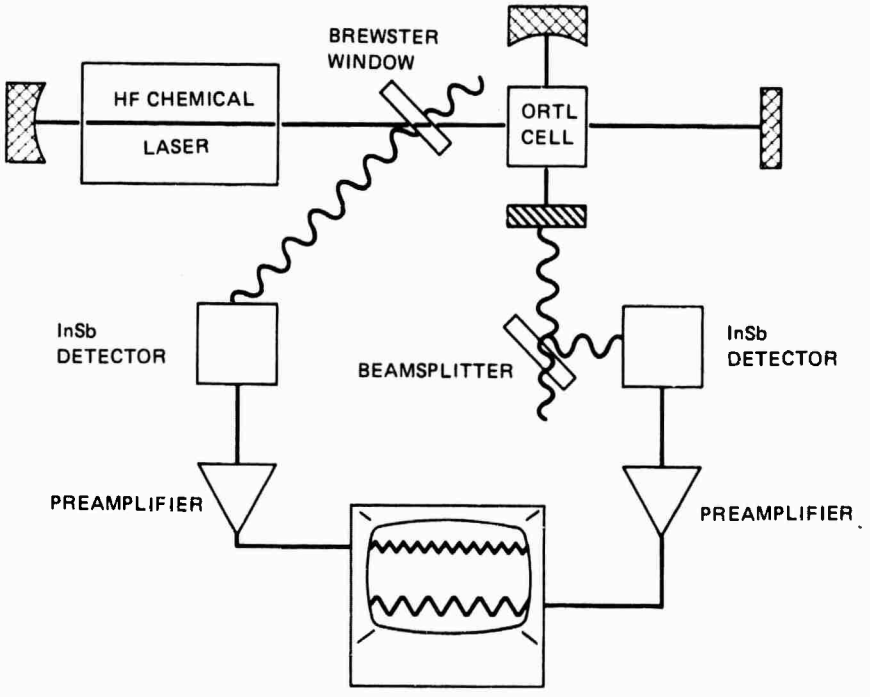

Figure 25. Intracavity configuration for chemical laser/ORTL dynamics study.

The ORTL cells were originally designed for extracavity experiments, where the beam from the pump laser was focused to give a small interaction zone. In the intracavity configuration the pumping beam is defined by the geometry of the chemical laser nozzle. For the intracavity cells, this resulted in the chemical laser irradiance impinging on the ORTL nozzle. To protect the nozzle, a pair of rectangular apertures was installed in the chemical laser resonator to confine the pump laser irradiance to 0.7 cm x 3 cm, and placed so that the irradiance did not strike the ORTL nozzle. This reduced the chemical laser resonator mode volume and consequently the power output.

The test configuration used for the extracavity temporal measurements is shown in Figure 24. The chemical laser output is sampled by a beamsplitter after leaving the resonator. A calibrated photoconductive indium antimonide detector/preamplifier with a frequency response of 200 KHz was used to monitor the chemical laser output, with the signal displayed on one channel of a storage oscilloscope. The ORTL output was sampled in the same fashion, with the signal displayed on the second channel of the oscilloscope. This permitted the simultaneous display of the instantaneous output of both the ORTL and the chemical laser. Varying the timebase of the oscilloscope permitted the convenient display of the amplitude variations at various frequencies. The intracavity configuration (Figure 25) was similar.

Prior to presentation of the results of the temporal measurements, the observed intracavity ORTL performance will be discussed. The measured parameters were: the outcoupled chemical laser power and its spectral distribution (outcoupled by the Brewster window), the chemical laser power coupled into the resonator mirrors, the power absorbed by the ORTL medium, and the ORTL power and spectral distribution. Data for the 3mm x 3 cm orthogonal cell are summarized in Table 7. All powers are in watts. The total extracted chemical laser power was approximately 300 watts, regardless of the ORTL loading. The power outcoupled by the Brewster window was 200 watts with no HF in the ORTL medium. This value was much higher than initially expected. With a calcium fluoride Brewster window in the laser resonator, the round-trip loss due to the window was less than 0.6 percent for the p-polarization, the estimated loss for the s-polarization was 40 percent. One would expect that the chemical laser

TABLE 7. POWER DISTRIBUTION FOR 3 MM X 3 CM INTRACAVITY EXPERIMENTS (PRESSURE = 76 TORR AND VELOCITY = 5 X 10^3 CM/SEC)

HF Mole Fraction	ORTL Output	Chemical Laser Power Absorbed in Mirrors	Outcoupled Power	Power Deposited in ORTL Gas	Extracted Chemical Laser Power
0.0	0	90	203	0	293
0.015	7.0	78	157	66	301
0.02	4.2	66	171	91	328
0.03	2.2	67	107	146	320
0.045	0	43	69	190	300

would be forced to oscillate only on the low-loss p-polarization, which has a total round trip loss (including mirror absorption) of 3.5 percent in the absence of an ORTL load. However, the chemical laser was also able to oscillate on the s-polarization with a total loss of 43 percent.

Measurement of the polarization of the output from the Brewster window confirmed that the s-polarization was lasing; more than 99 percent of the Brewster window power was s-polarized. The output beam had the dimensions of the intracavity apertures, 0.7 cm x 3 cm. The output power, (200 watts), the outcoupling fraction (40 percent), and the area (2.1 cm^2), yield an intracavity intensity of 480 watts/cm^2. The resonator mirrors have a total absorption of 3 percent, and so absorb 15 watts from the s-polarization. Thus the total extracted power in the s-polarization was 215 watts.

The total power absorbed by the chemical laser mirrors, 90 watts, is composed of both the s- and p-polarizations. Since the s-polarization accounts for 15 watts, the p-polarization is responsible for 75 watts. The circulating intensity in the p-polarization is therefore 2380 watts/cm^2. Note that if the p-polarization were to occur to the exclusion of the s-polarization, or if the Brewster window were absent, the full 300 watts would be deposited in the resonator mirrors, a 3 percent loss, giving an intracavity irradiance of 9500 watts/cm^2. This would result in greatly improved performance.

An additional complication occurs when the addition of an ORTL load to the chemical laser resonator increases the total losses for both polarizations. The power in the s-polarization, where losses are 43 percent in the absence of an ORTL load, is reduced substantially, while the p-polarization is relatively unaffected. This is shown in Table 7, where the power deposited in the chemical laser mirrors is predominantly from p-polarization and the Brewster window power is s-polarization. Thus the distribution of the chemical laser power among different losses is a function of the ORTL loading.

The efficiency of coupling into the ORTL medium is also different for the two polarizations. For the s-polarization, it is impossible for the ORTL to compete effectively against the large resonator losses. For an ORTL load averaging 10 percent round trip absorption, the percentage of extracted chemical laser power which is coupled into the ORTL medium would only be 18 percent. On the other hand, the p-polarization with a 10 percent load absorbs 75 percent of the extracted power. However, the high round trip loss of 13.5 percent reduces the intracavity irradiance to 617 watt/cm^2, which decreases the conversion efficiency. Because of the high overall losses and resultant low intracavity flux, the intracavity power and efficiency were very low. Expected improvement would come from removing the high-loss Brewster window and replacing it with an aerodynamic window, so that the complicated polarization characteristics of the chemical laser could be eliminated.

The spectral distribution of the pump laser as a function of HF mole fraction in the ORTL cell is shown in Figure 26. J-values of the lasing transitions were shifted toward higher values as HF mole fraction increased. The presence of HF loading increases the relative loss on low J transitions, as these are more strongly absorbed, which in turn leads to lasing on lower loss transitions with higher J-values. ORTL output spectra, illustrated in Figure 27, show a trend similar to that in extracavity cases (see section 2).

To compare extracavity and intracavity ORTL amplitude variations at comparable ORTL power levels, the chemical laser power was adjusted to provide the same pump intensity. Pumping intensity for both the extracavity

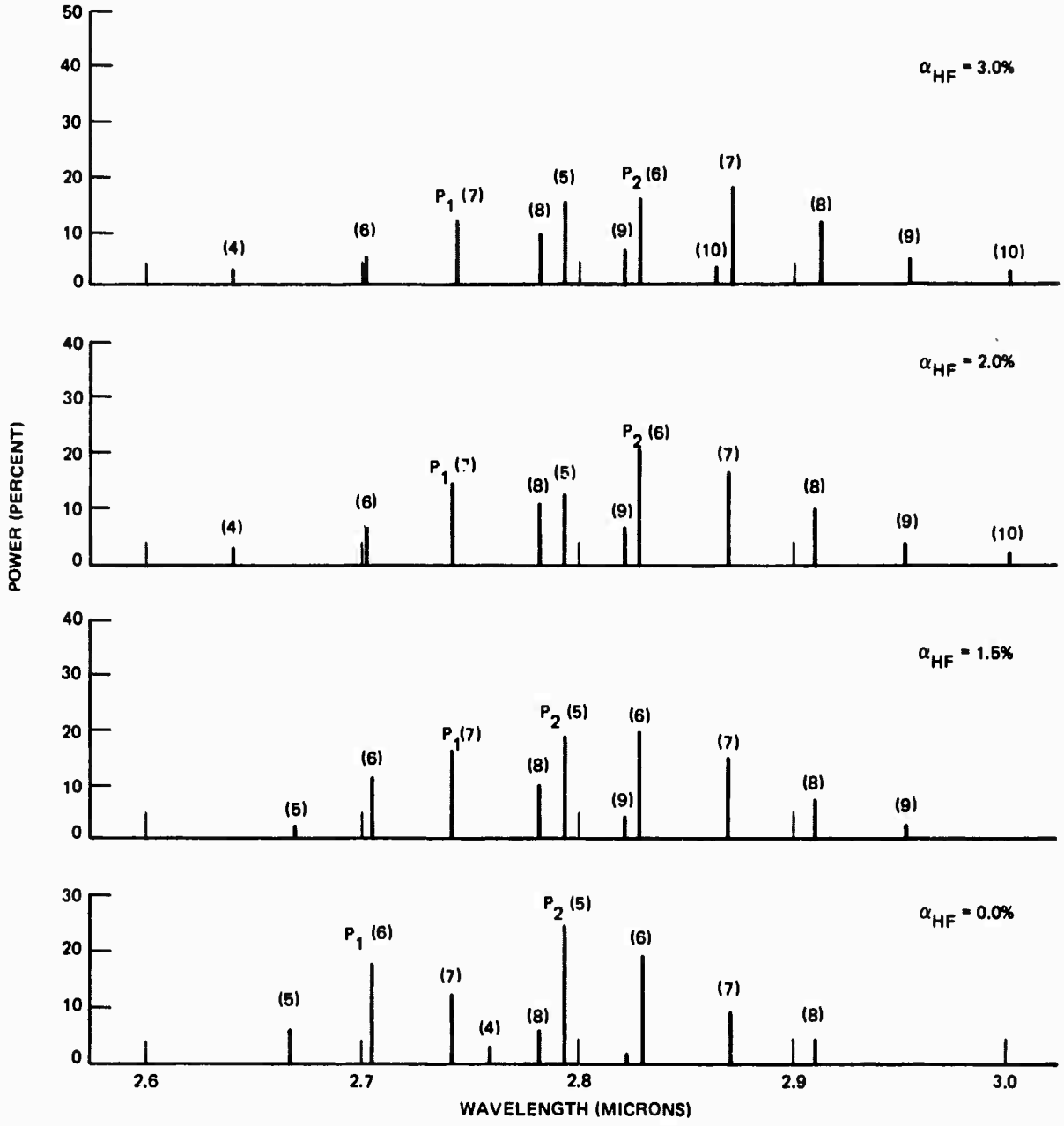

Figure 26. Chemical laser spectra at various HF ORTL concentrations.

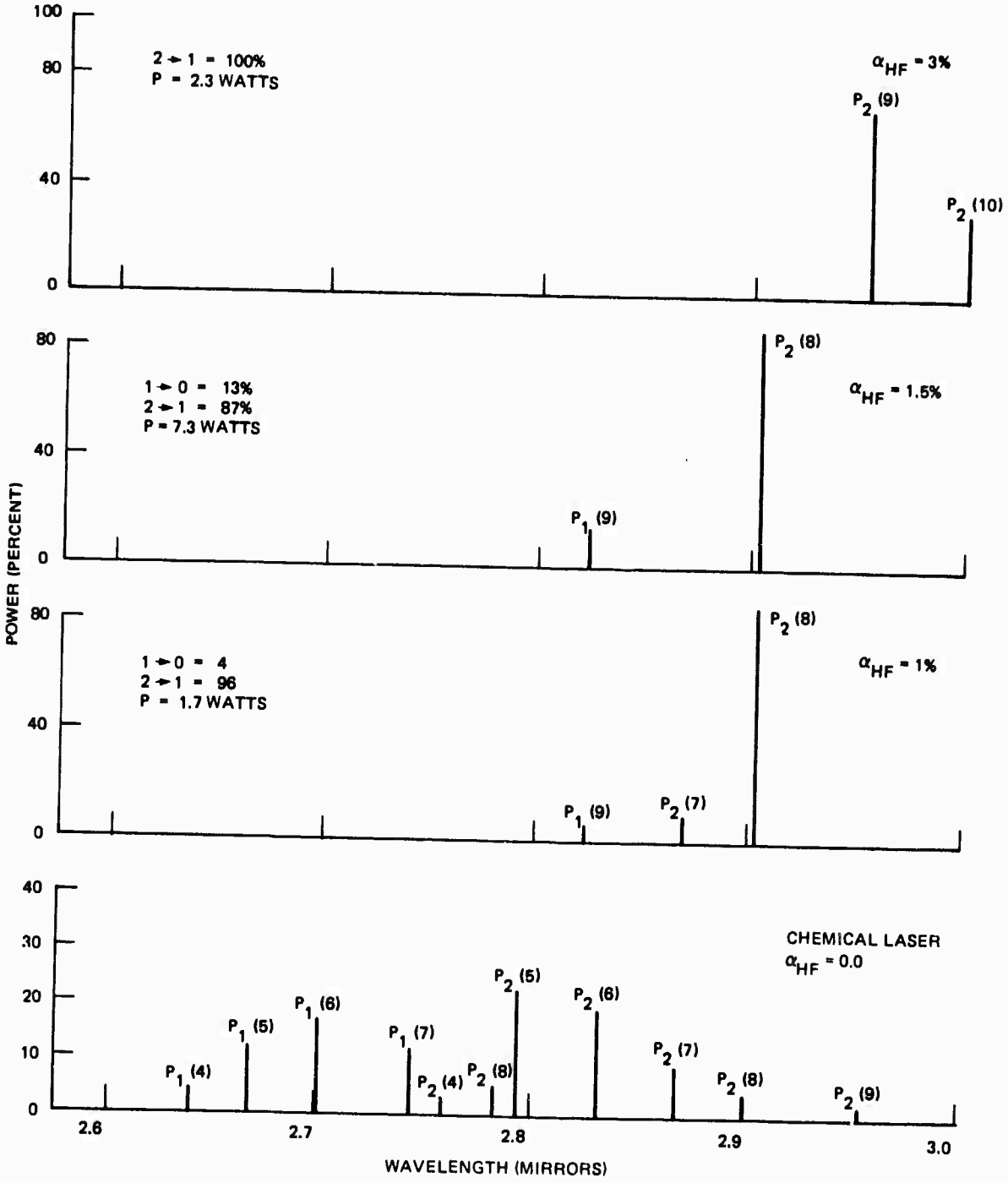

Figure 27. ORTL output spectra — intracavity experiments.

and intracavity cases was approximately 500 watts/cm^2. ORTL output was comparable for both cases.

Typical data for a series of extra- and intra-cavity amplitude measurements are presented in Figures 28 to 33. This data was taken using the 3mm x 6 cm rotated ORTL cell. Figure 28 shows the output from an efficient extracavity ORTL. It is presented as a standard for comparison to intracavity cases. Figure 29 is from an extracavity ORTL near threshold. It is presented to illustrate the increased temporal variations near threshold, and also the inverse correlation to the pump laser power, discussed below. Figures 30 to 33 show results from intracavity conditions with various mole fractions of HF, which provide up to 40 percent of the total load on the chemical laser.

Figure 34 shows that the multi-line chemical laser amplitude fluctuations are unaffected by the addition of an intracavity ORTL. The noise is thought to be due to acoustic noise from supersonic mixing dynamics in the chemical laser cavity.

Figure 35 shows that the ORTL amplitude fluctuations at less than 3 kHz are larger than that of the pumping laser. In the best extra- and intracavity cases, the ORTL fluctuations are approximately 40 percent larger than those of the chemical laser. In fact, the intracavity configuration exhibits smaller fluctuations. These ORTL conditions also resulted in the highest ORTL output power.

Figures 29, 30, and 32 show that the ORTL power can vary oppositely to the total chemical laser power. (This effect is much reduced, or absent, in Figures 28 and 31, which are optimized extra- and intra-cavity cases.) This effect is ascribed to variations in the chemical laser spectral distribution on the acoustic timescale in an inverse relation to total multiline power. The medium HF intracavity ORTL (Figure 31) is less affected by these variations than are the cases with either a higher or lower mole fraction of HF in the ORTL medium. Where total HF number density is low, optimum J-distribution is necessary to produce an adequate population of excited states to sustain inversion. Figure 29, with an extremely low concentration of HF, shows this to the largest extent; it is at threshold. Figure 30, an intracavity ORTL with less than optimum HF concentration, shows this to a lesser extent.

With high HF concentration (Figure 32) the ORTL has begun to load the chemical laser significantly, changing the J-distribution by decreasing the lower J transitions, and also decreasing the proportion of the V = 1→0 transition in the total laser power. The efficiency of pumping with this spectral distribution is lower. The intracavity irradiance is also lower, and the sensitivity to J-distribution is thus increased. The medium HF condition (Figure 31), is affected by neither of these effects to a large extent.

The significant results of the experiments reported above are:

1. The intracavity ORTL had no significant effect on the multi-line chemical laser amplitude fluctuation at ORTL loads up to 40 percent of the total losses. Larger losses were not investigated.
2. The amplitude fluctuation of the ORTL output was not dependent on whether the ORTL cell was extra- or intra-cavity.
3. In both the extra-cavity and intra-cavity cases. the ORTL output had greater amplitude fluctuations than the multi-line chemical laser.
4. The inverse correlation between the chemical laser power and the ORTL output, observed in both the extracavity and intracavity configurations, suggests that chemical laser J-distribution is varying in a sense opposite to the total power. In other words. when the chemical laser is producing high power it does so with a poor J-distribution for ORTL pumping. The observation of this phenomenon in the extracavity configuration shows that this chemical laser fluctuation is not produced by the ORTL cell.

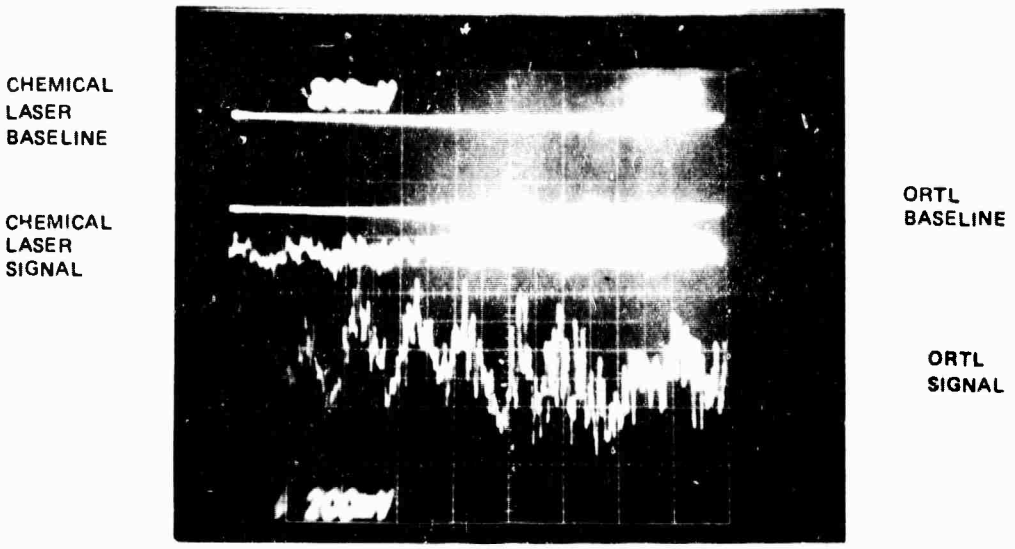

a. 10 msec/div

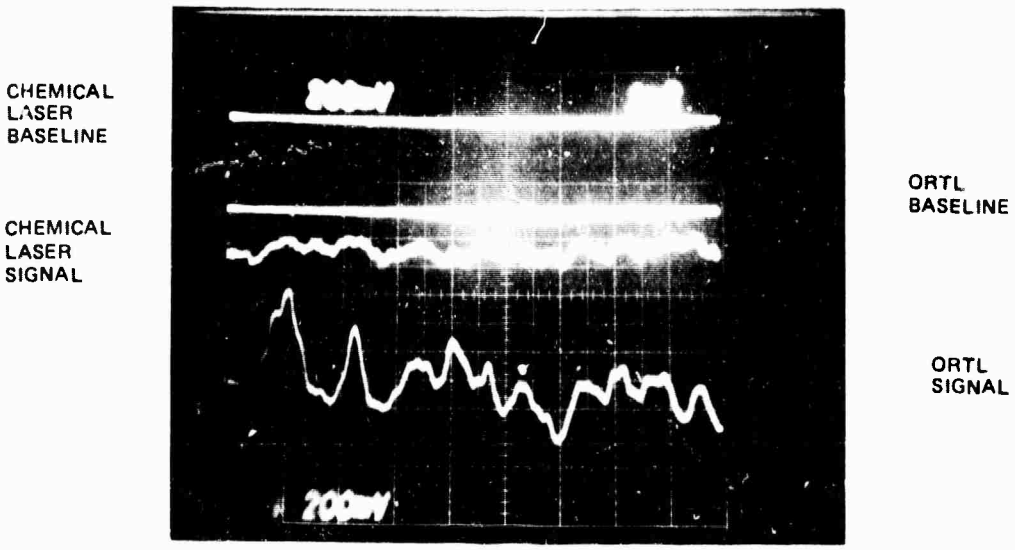

b. 1 msec/div

Figure 28. Extracavity ORTL temporal characteristics.

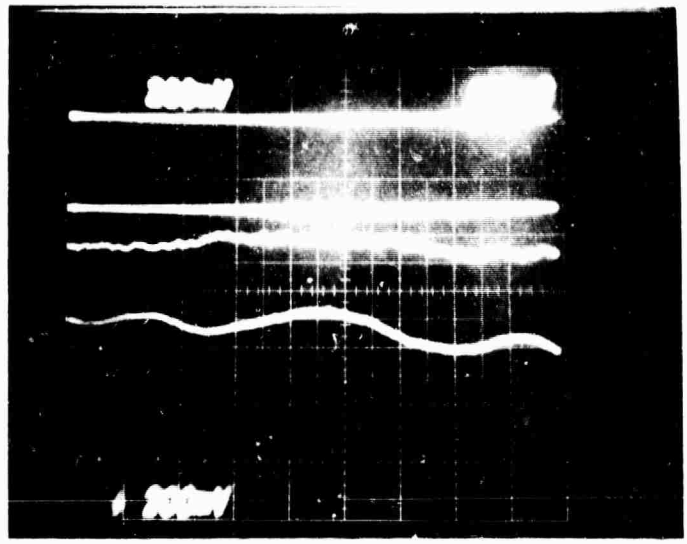

c. 100 μsec/div

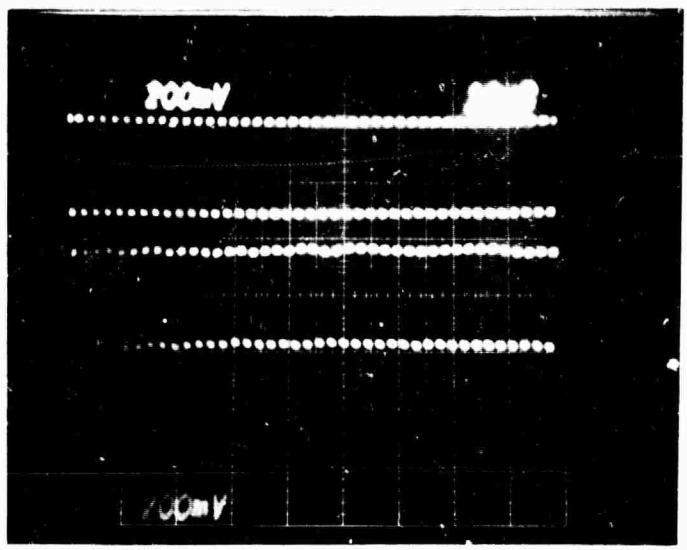

d. 10 μsec/div

PRESSURE	76 TORR (0.1 ATMOSPHERE)
MOLE FRACTION HF	0.005
ORTL POWER	0.4 WATTS
PUMP INTENSITY	500 W/CM^2

Figure 28. (Cont'd)

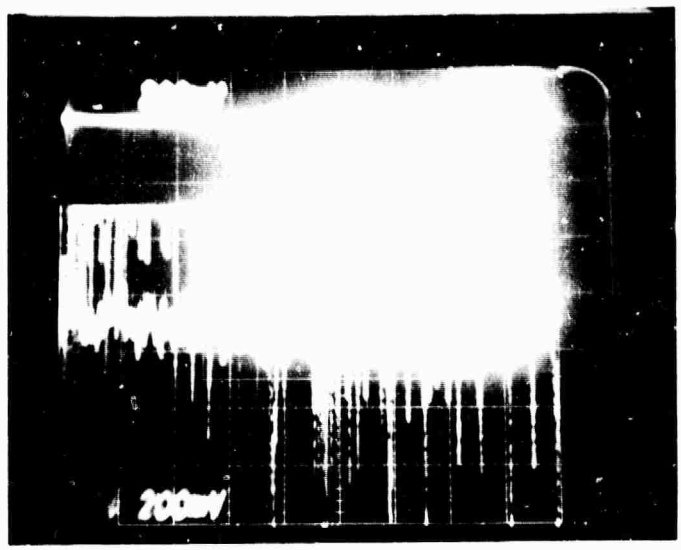

a. 10 msec/div

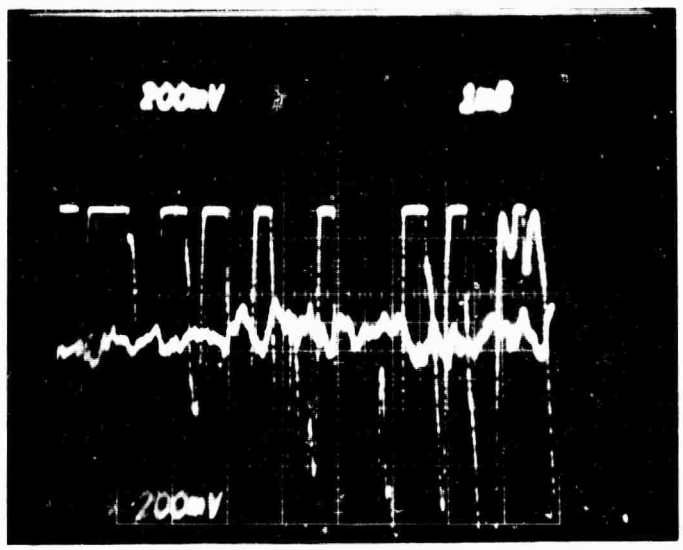

b. 1 msec/div

Figure 29. Extracavity ORTL temporal characteristics near threshold.

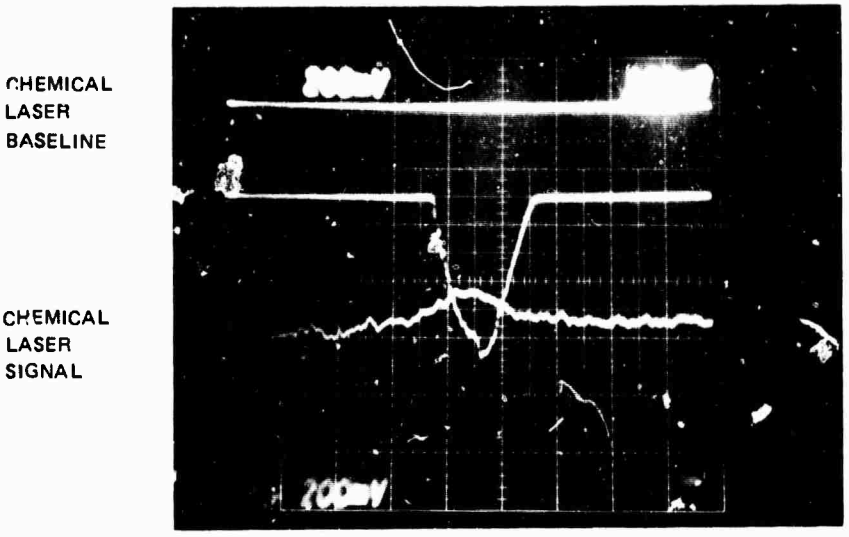

c. 100 μsec/div

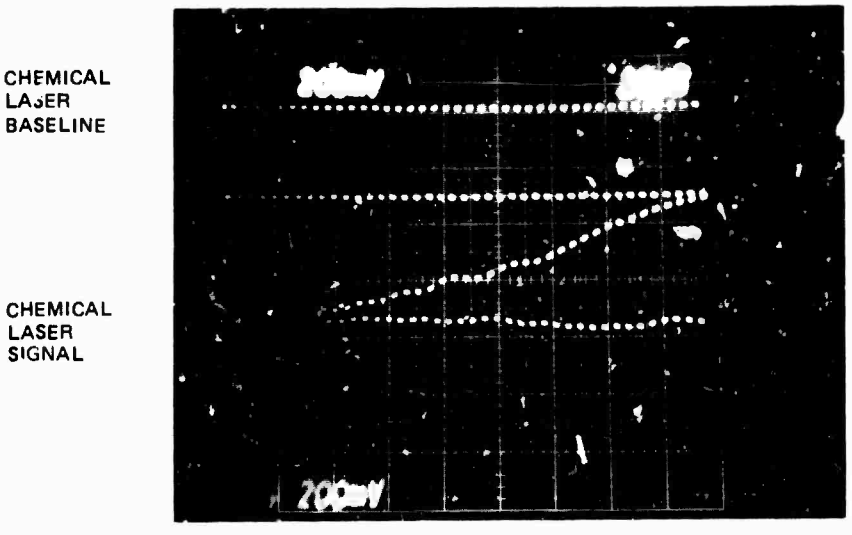

d. 10 μsec/div

PRESSURE	76 TORR (0.1 ATMOSPHERE)
MOLE FRACTION HF	0.0006
ORTL POWER	0.20 WATTS
PUMP INTENSITY	750 W/CM^2

Figure 29. (Cont'd)

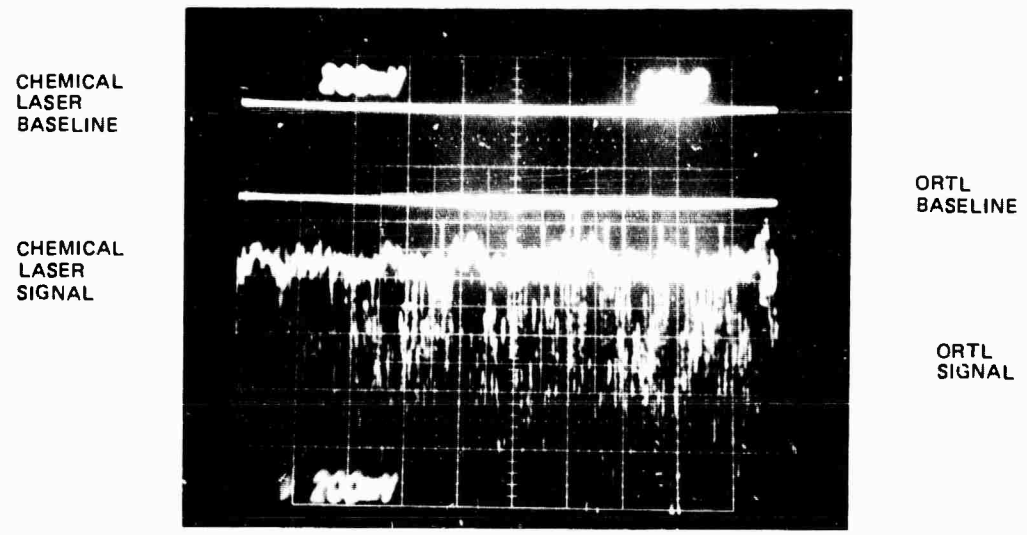

a. 10 msec/div

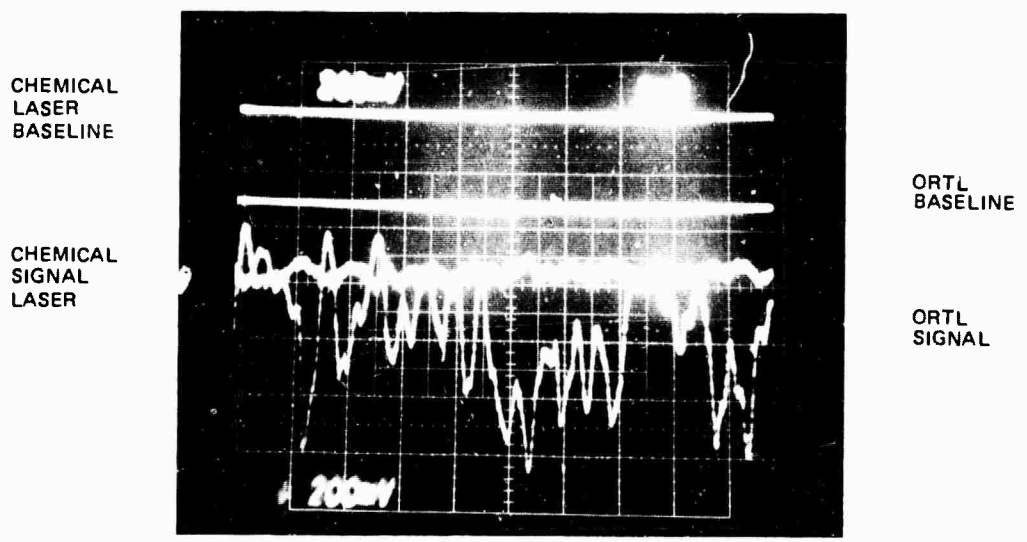

b. 1 msec/div

Figure 30. Intracavity ORTL temporal characteristics (low HF).

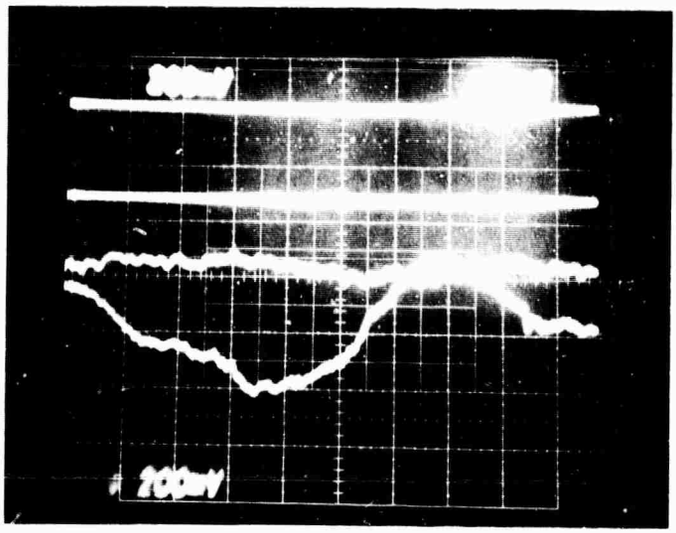

c. 100 μsec/div

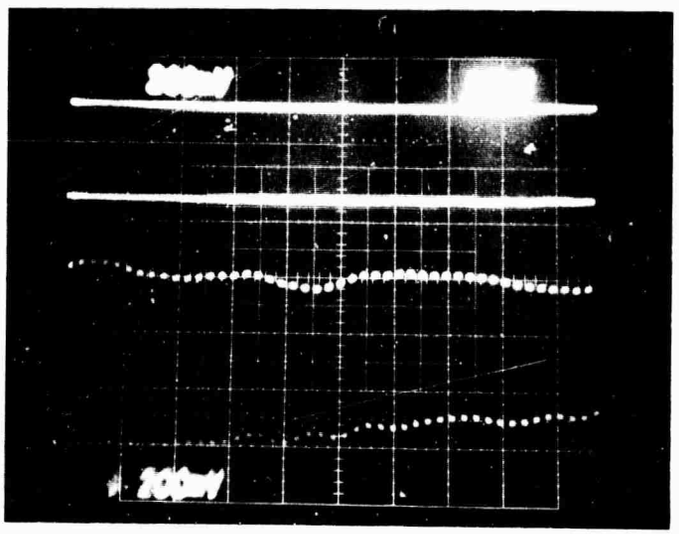

d 10 μsec/div

PRESSURE	77 TORR (0.1 ATM)
MOLE FRACTION HF	0.001
LINES OBSERVED	P_1 (7) (50%); P_2 (7) (50%)
PERCENTAGE OF LOAD ON CHEMICAL LASER	7.3
ORTL POWER	0.53 WATTS
PUMP INTENSITY	500 W/CM^2

Figure 30. (Cont'd)

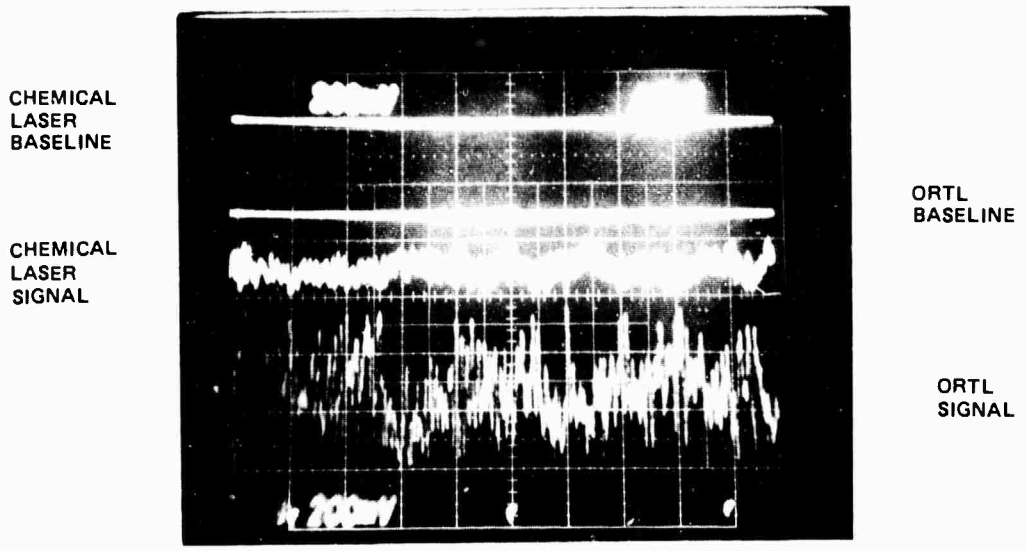

a. 10 msec/div

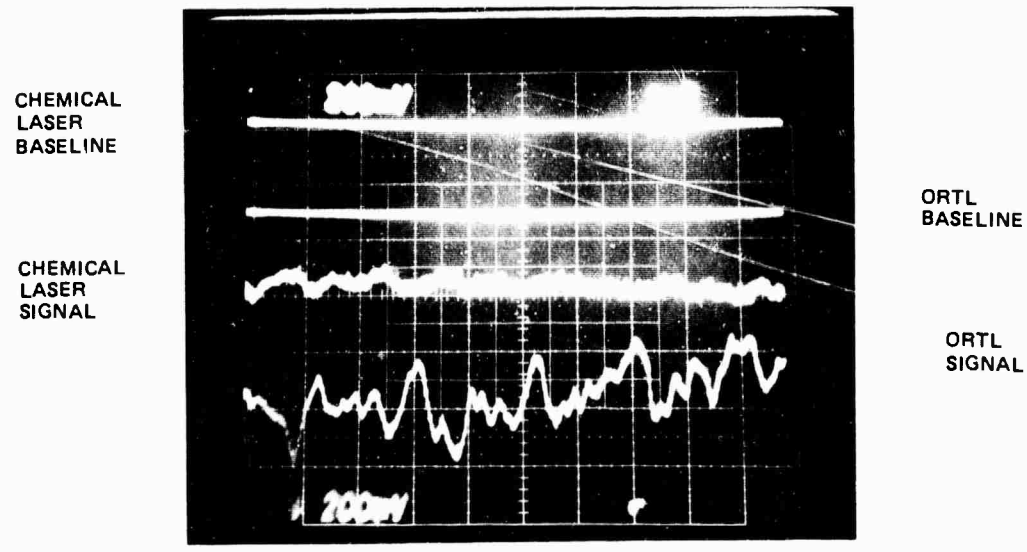

b. 1 msec/div

Figure 31. Intracavity ORTL temporal characteristics (medium HF).

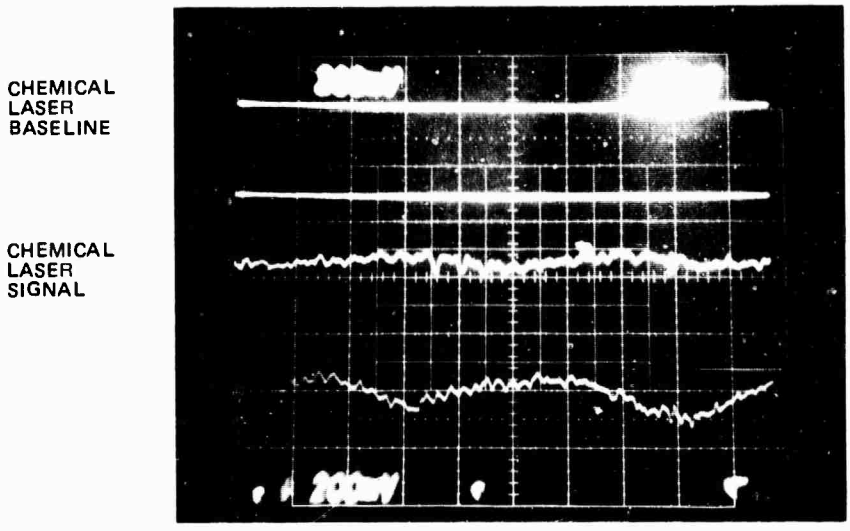

c. 100 μsec/div

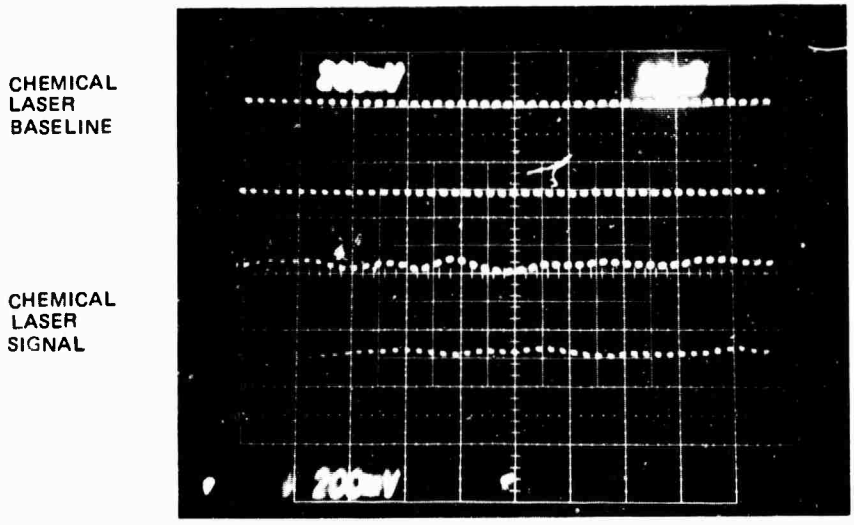

d. 10 μsec/div

PRESSURE	77 TORR (0.1 ATMOSPHERE)
MOLE FRACTION HF	0.003
LINES OBSERVED	P_1 (8) (20%), P_2 (7) (80%)
PERCENTAGE OF LOAD ON CHEMICAL LASER	16.3
ORTL POWER	0.76 WATTS
PUMP INTENSITY	500 W/CM^2

Figure 31. (Cont'd)

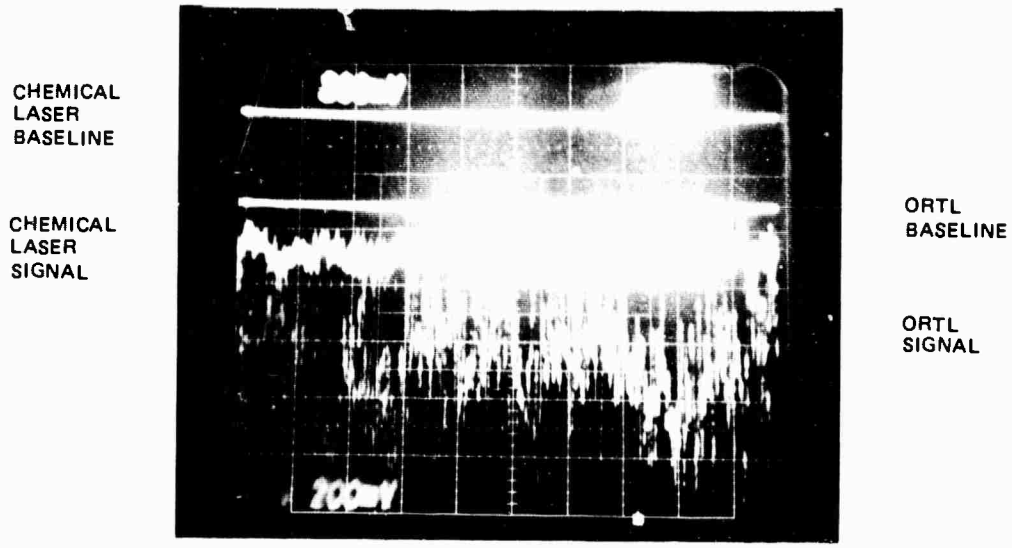

a. 10 msec/div

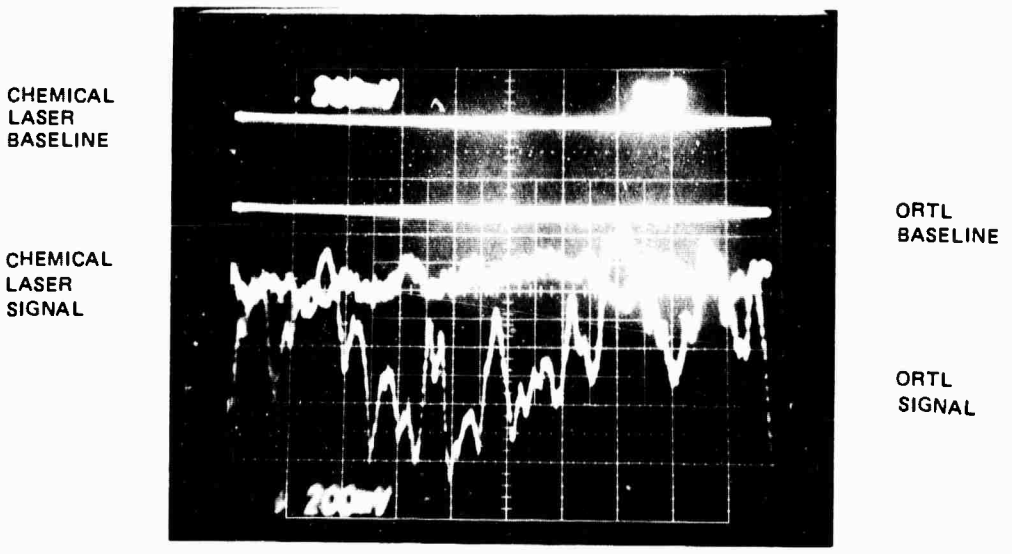

b. 1 msec/div

Figure 32. Intracavity ORTL temporal characteristics (high HF).

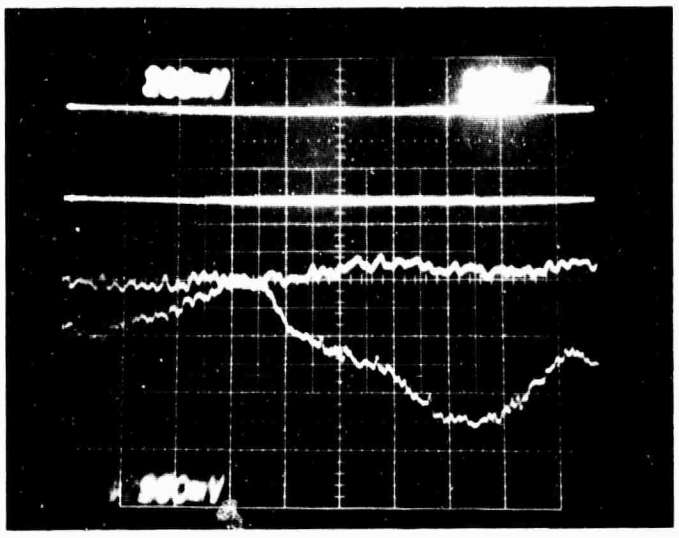

c. 100 μsec/div

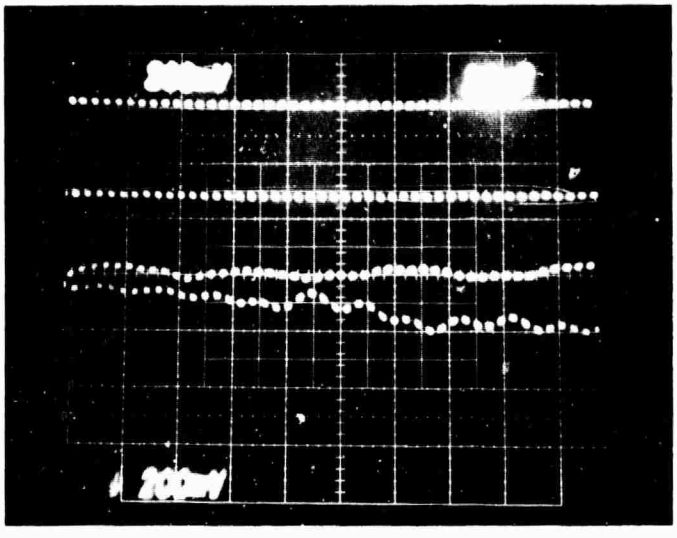

d. 10 μsec/div

PRESSURE	78 TORR (0.1 ATMOSPHERE)
MOLE FRACTION HF	0.01
LINES OBSERVED	P_2 (7) (100%)
PERCENTAGE OF LOAD ON CHEMICAL LASER	40.9
ORTL POWER	0.29 WATTS
PUMP INTENSITY	425 W/CM^2

Figure 32. (Cont'd)

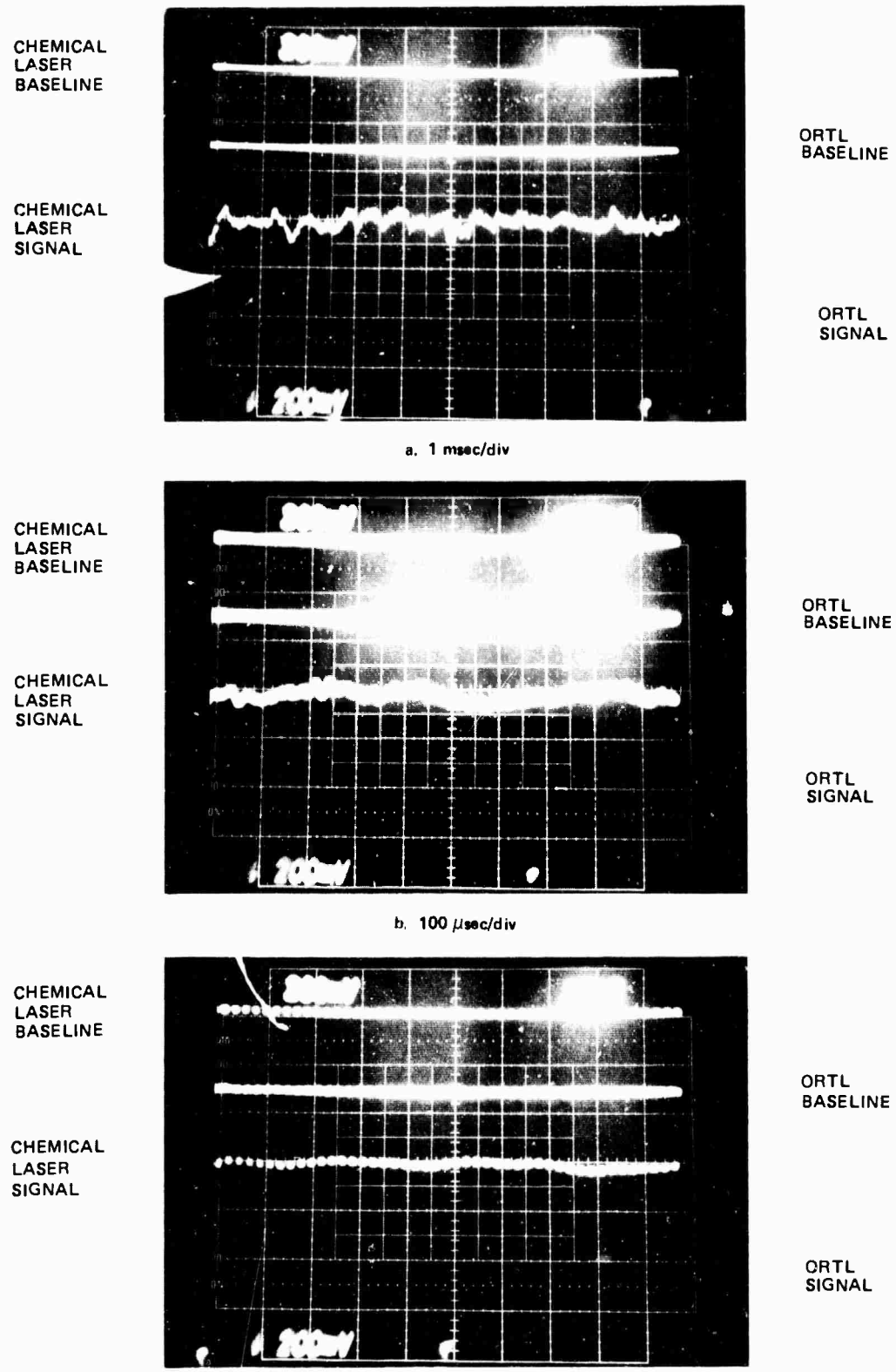

Figure 33. Intracavity ORTL configuration – chemical laser temporal characteristics (no HF).

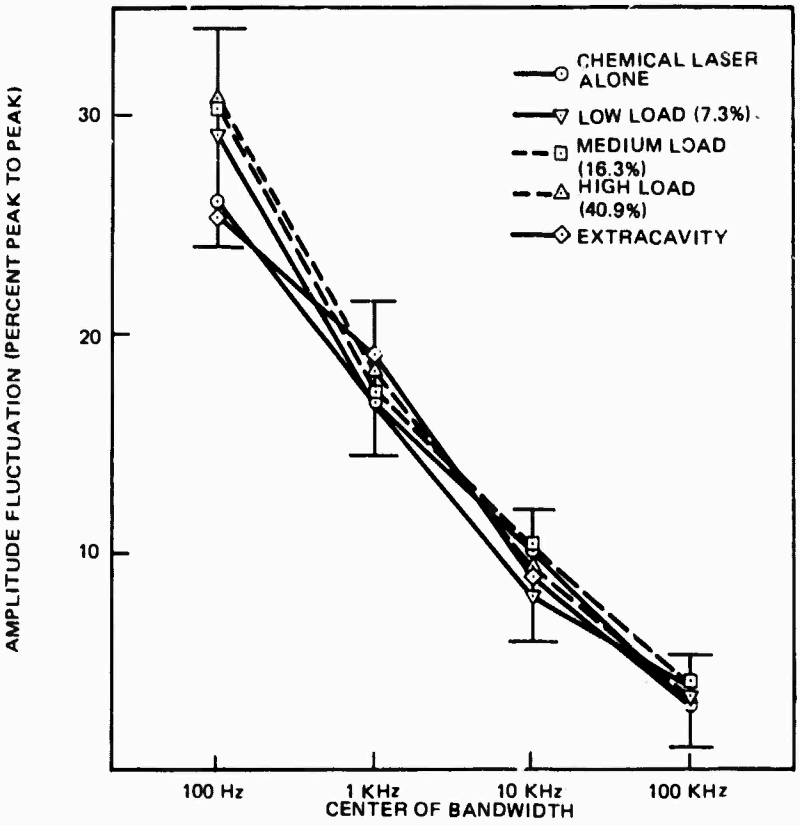

Figure 34. Frequency dependence of chemical laser amplitude fluctuations.

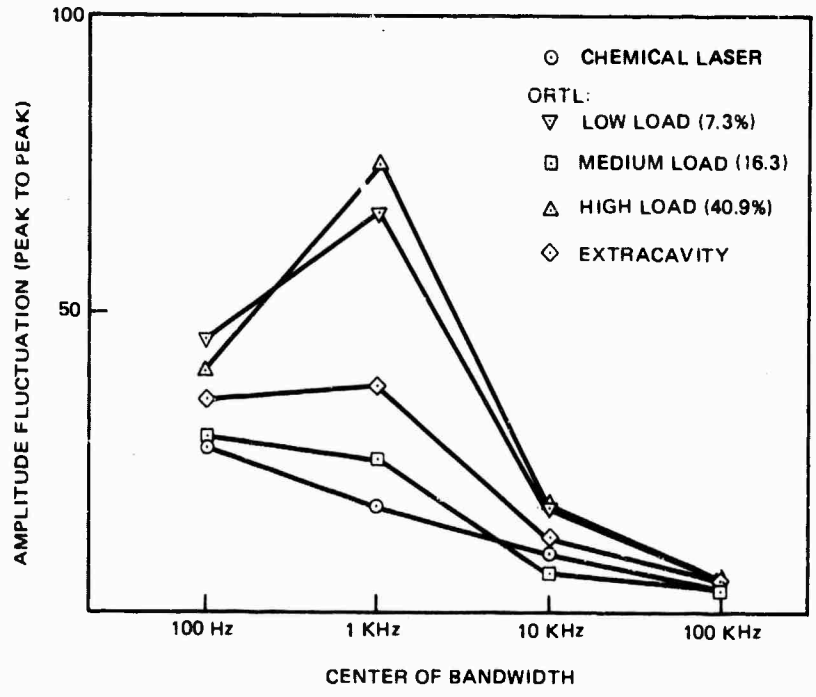

Figure 35. Frequency dependence of ORTL and chemical laser amplitude fluctuations.

4.0 BEAM QUALITY

ORTL beam quality was determined by measuring the far field diffraction pattern of the output beam. A monochromatic, uniform intensity, plane wave incident on a circular limiting aperture forms an Airy pattern in the far field. The Airy pattern is characterized by a central disc with surrounding rings of rapidly decreasing intensity. The fraction of the power in the central disc, and the radius of the disc, are well known; 83.5 percent of the transmitted power will fall within a diameter $2.44\ R\lambda/D$, where λ is the wavelength of the light, D is the diameter of the diffracting aperture and R is the distance to the observation plane. This provided the standard of comparison for experimental far field "power-in-the-bucket" results. Varying apertures were placed in the far field observation plane and the transmission through these "buckets" measured. Beam quality can then be specified by the square root of the ratio of the ideal power transmitted by an aperture to the measured power transmitted, when the aperture has the diameter of the Airy disc. Beam quality is then expressed as a multiple, n, of a diffraction limited beam, where

$$n^2 = \frac{\text{power (ideal)}}{\text{power (experimental)}}$$

Alternatively, the approach to an Airy pattern may be judged by the radial distribution of the power in the far field as measured by a series of apertures.

The experimental configuration for the beam quality measurement is shown in Figure 36. In this experiment the ORTL resonator is designed to oscillate in a single mode. The rotated ORTL cell was used with a semi-confocal resonator consisting of a 3 meter radius spherical mirror facing a flat 1.9 percent outcoupler at a separation of 150 cm. The gain medium was defined by the ORTL nozzle, 6 cm x 0.3 cm and by the height of the pumping laser radiation, which was focused to 0.35 cm. An internal

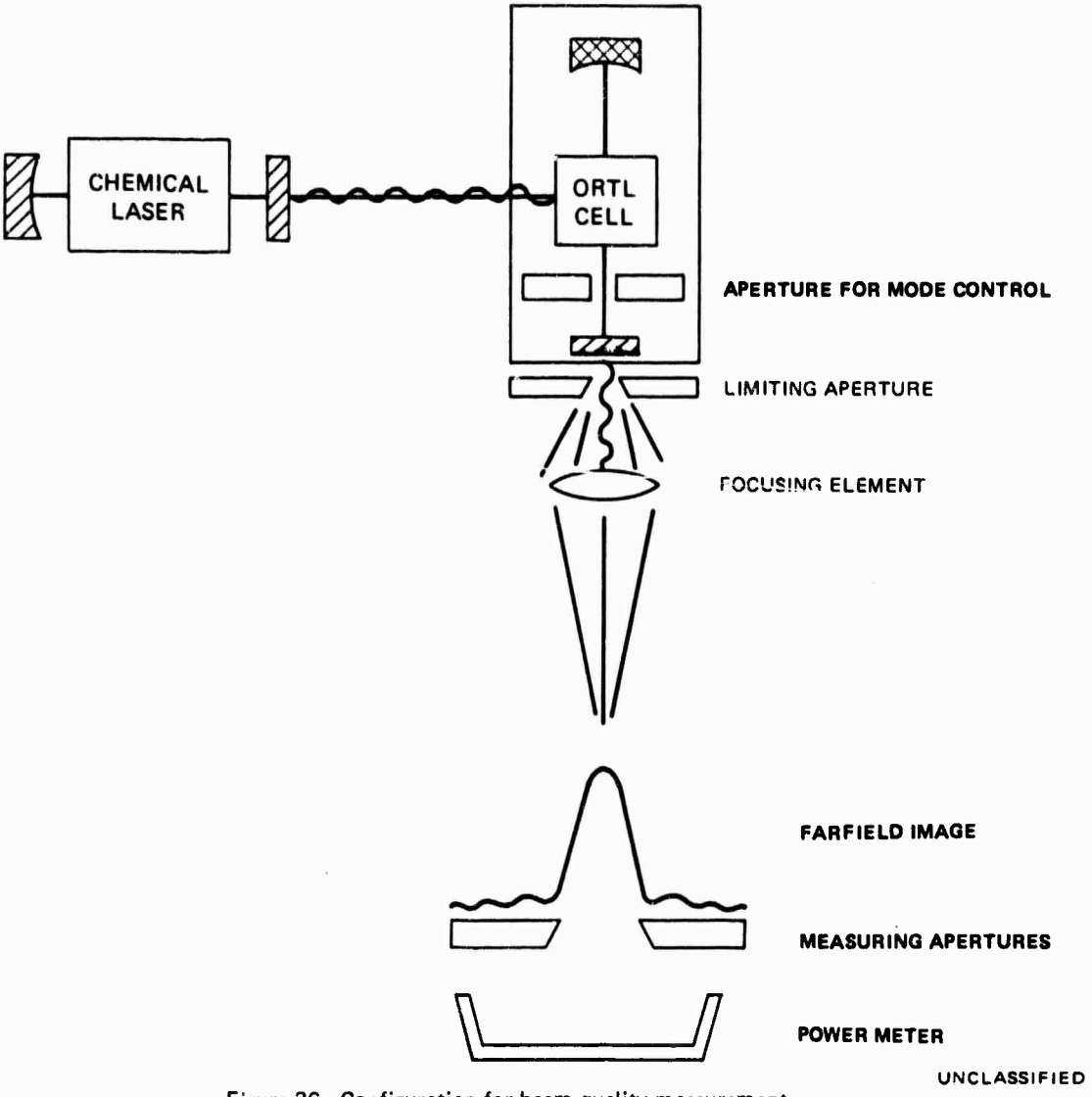

Figure 36. Configuration for beam quality measurement.

aperture of 0.40 cm diameter was used to eliminate all but the lowest order mode. The output of this simple resonator is expected to be a Gaussian plane wave with the diameter at the 1/e intensity points equal to 0.24 cm. Thus, most of the output ORTL power was transmitted through the 0.24 cm limiting aperture, which was carefully centered on the output beam by maximizing the power transmitted through it. The output beam was then focused by a three meter radius mirror located 30 cm from the limiting aperture.

The output of the resonator is initially a plain wave, but Fresnel diffraction results in a divergent beam at the focusing mirror. The radius of curvature R_1 at this element was 780 cm. The distance R_2 from the mirror to the plane in which the far field was simulated is given by

$$\frac{1}{R_2} = \frac{1}{f} - \frac{1}{R_1}$$

where f is the focal length of the mirror. In this case, a 150 cm focal length mirror was used and R_2 was 186 cm. The diameter of the Airy disc was 0.58 cm. In this focal plane, a series of apertures (or "buckets") of various diameters ranging from 0.15 to 1.0 cm were carefully positioned by maximizing the power transmitted through them. The fractional power transmitted by each of these second apertures was measured by a pyroelectric radiometer and the results are shown in Figure 37.

Single line operation was obtained by operating the ORTL cell at high HF mole fraction; this also resulted in a much larger absorption of pumping laser power and larger heating of the ORTL medium. The results are shown in Figure 38. Figures 37 and 38 both show beam quality of better than 1.05 times diffraction limited, this being the lower limits of the error bars. The data includes a range of ORTL temperature rises over which we have demonstrated closed-cavity overall efficiencies of 23 to 27 percent. Although the beam quality measurements show diffraction limited output, it should be noted that even severe density variations in the short ORTL medium would not result in far field effects.

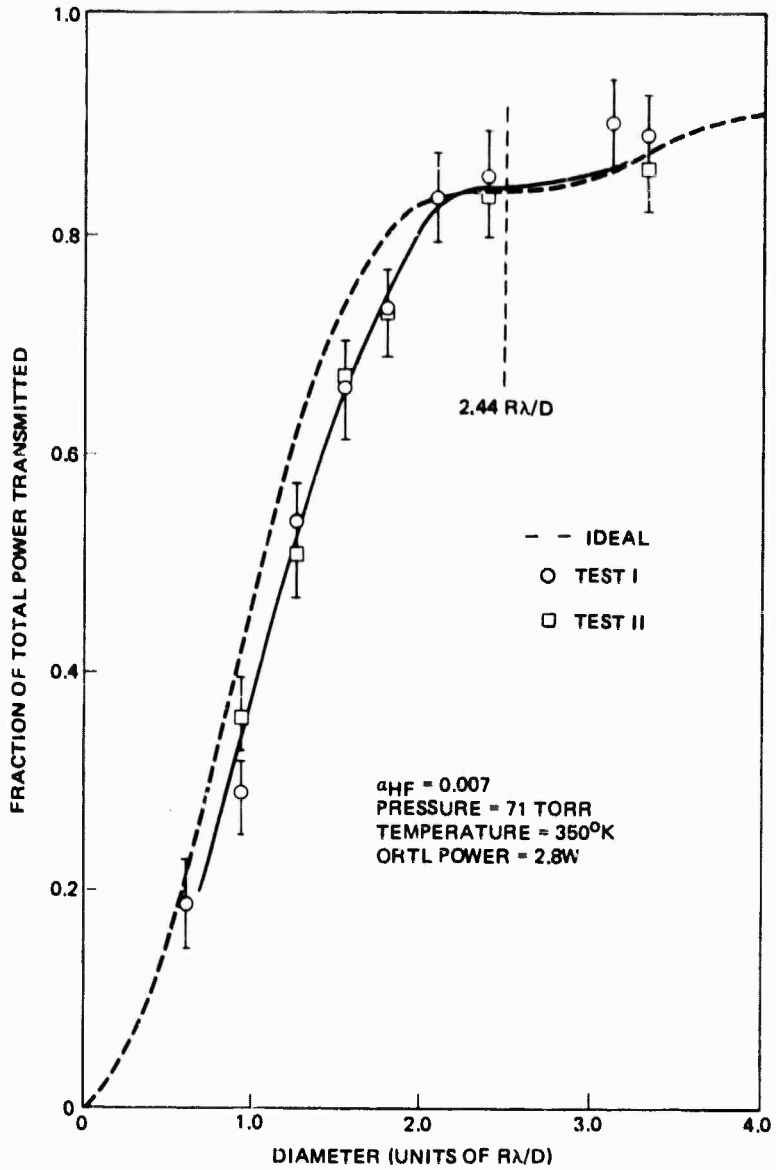

Figure 37. Multi-line beam quality measurement results.

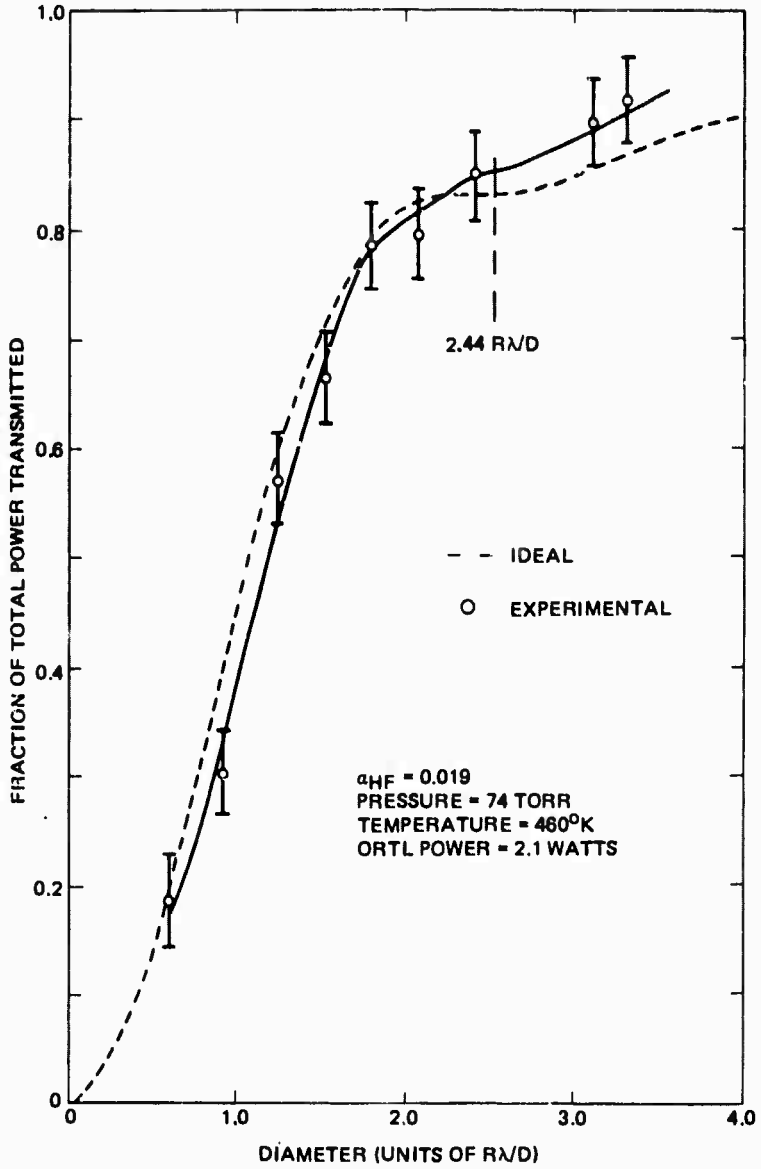

Figure 38. Single-line beam quality measurement results.